Journal of Oceanography (2019) 75:375–393
https://doi.org/10.1007/s10872-019-00514-9

REVIEW

A note on estimating eddy diffusivity for oceanic double-diffusive convection

Haruka Nakano[1] · Jiro Yoshida[1]

Received: 25 August 2018 / Revised: 20 April 2019 / Accepted: 24 April 2019 / Published online: 21 May 2019

Abstract
In this note, we provide an overview of the theoretical, numerical, and observational studies focused on oceanic eddy diffusivity, with an emphasis on double-diffusive convection (DDC). DDC, when calculated using the turbulent kinetic energy (TKE) equation, produces a negative diffusion of density. A second-moment closure model shows that DDC is effective within a narrow range. Other parameterizations can use in the actual sea, but improvements are still needed. Mixing coefficients referring to mixing efficiency are key factors when distinguishing DDC from conventional turbulence. Here, we show that measurements involving the gradient Richardson number, the buoyancy Reynolds number, and density ratio play a crucial role in determining eddy diffusivity in the presence of DDC. Therefore, deployment of a microstructure profiler together with either an acoustic Doppler current profiler (ADCP), lowered ADCP, or electromagnetic current meter is essential when measuring eddy diffusivity in the ocean's interior.

Keywords Double-diffusive convection · Mixing coefficient · Mixing · Turbulence · Eddy diffusivity · Kinetic energy dissipation rate · Density ratio · Gradient Richardson number · Parameterization

1 Introduction

Microstructures resulting from conventional turbulence (CT) and double-diffusive convection (DDC) are among the many noteworthy physical processes occurring in the ocean. Although the rates of microstructure occurrence and their effects are gradually being revealed, more complete information about the occurrence of microstructures remains unknown. A better understanding of oceanic microstructures will provide value to multiple fields and may help in answering some outstanding questions in climatic modeling, water mass modification, and oceanic nutrient distribution processes.

CT and DDC are related to large-scale oceanic processes. For example, internal wave (IW) breaking can produce significant amounts of turbulence (e.g., Polzin et al. 1997). DDC occurring at $\sim$ 400 db generates North Pacific Intermediate Water (Talley and Yun 2001) and leads to intrusions in the subsurface layer off the Sanriku Coast of Japan (e.g., Nagata 1970; Nagasaka et al. 1999). Taken together, studies on microscale mixing [$\sim O(10^{-2})$ m] are strongly correlated with large-scale processes (e.g., meridional circulation: $\sim O(10^{3})$ m, intrusion and IWs: $\sim O(10^{2})$ m; Munk 1966; Bryan 1987; Gargett and Holloway 1992; Karl 1999). Nonetheless, the effects of DDC have been historically ignored in scientific study.

One reason why DDC has been ignored is the shortage of empirical knowledge typically obtained through observation. The opportunity for observations is limited because DDC is known to occur in areas such as shallow regions with commercial usage or in polar regions (e.g., Hirano et al. 2010). Moreover, limited ship time for observation and high cost of the microstructure profiler interrupt microstructure observations. Difficulties in handling microstructure data also exist. In addition, the areas surveyed for the detection of microstructures have incomplete coverage because the spatiotemporal scales of microscale

✉ Haruka Nakano
hnakan2@kaiyodai.ac.jp

Jiro Yoshida
jiroy@kaiyodai.ac.jp

[1] Faculty of Marine Science, Tokyo University of Marine Science and Technology, Konan 4-5-7, Minato-ku, Tokyo 108-8477, Japan

processes are smaller than those detected by routine observations.

In order to compensate for the difficulties mentioned above, parameterizations of eddy diffusivities and kinetic energy dissipation rates have been developed using the conductivity temperature depth (CTD) profiler, lowered ADCP (LADCP), and other common oceanic instruments for hydrographic data collection. However, at its current state, the parameterization is not completely developed, because the methods are based on certain limitations. Nearly all of the parameterization concerns deal with shear-driven turbulence (CT), which is due to IWs. When the velocity shear is superior (Kunze 1990), DDC coexists with CT; nevertheless, DDC has been ignored in the parameterization. Parameterizations of DDC are carried out using laboratory experiments and direct numerical simulations (DNS). This means that a comparison focusing on DDC with microstructure data is still required. Therefore, a more precise parameterization is required for future microstructure studies.

The rest of this overview is structured as follows. We summarize previous studies on eddy diffusivity and present the results of DDC parameterization in oceanic turbulent mixing. DDC in the turbulent kinetic energy (TKE) equation is discussed in Sect. 2. Parameterization of eddy diffusivity using a second-moment closure (SMC) model is described in Sect. 3. Other types of DDC parameterizations in numerical simulations are described in Sects. 4 and 5. Key points regarding the eddy diffusivity estimation with measurement data are described in Sect. 6. Finally, concluding remarks are presented in Sect. 7. Details regarding the turbulent kinetic energy (TKE) equation, laboratory flux laws, SMC model, and relevant terminologies are presented in Appendices A–D, respectively.

2 Eddy diffusivity with turbulent kinetic energy equation and flux laws

DDC has two forms of convection: salt finger convection (SF) and diffusive convection (DC). DDC is characterized by the density ratio $R_\rho = \alpha \frac{\partial \bar{T}}{\partial z} \Big/ \beta \frac{\partial \bar{S}}{\partial z}$, which is the ratio of the background density gradient due to temperature to that due to salt, where α and β are the expansion and contraction coefficients for heat and salt, respectively (Eq. 77). $\frac{\partial \bar{T}}{\partial z}$ and $\frac{\partial \bar{S}}{\partial z}$ represent the background temperature and salt gradients, respectively. Generally, SF is considered active when $1 < R_\rho < 2$, and DC is considered active when $0.5 < R_\rho < 1$ (e.g., Inoue et al. 2007). When CT is weak and DDC is active, the density is transported downward because of the difference in molecular diffusivity for heat and salt; therefore, the eddy diffusivities for salt K_S, heat K_T, and density K_ρ are not equal to one another (see Appendices A and B). This characteristic is unique to DDC.

Consider the steady-state TKE equation for SF without background velocity shear (refer to Eq. 67). The balance equation between the dissipation rate of the TKE ε (refer to kinetic energy dissipation rates) and the energy production via buoyancy flux J_b is as follows:

$$0 = \varepsilon + g\frac{\overline{\rho' w'}}{\bar{\rho}} = \varepsilon + J_b. \tag{1}$$

Thus, J_b should be negative for DDC. From Eq. (82), and under the Boussinesq approximation ($\bar{\rho} = \rho_0$), J_b can be written as

$$J_b = g\frac{\overline{\rho' w'}}{\rho_0} = g\frac{F_\rho}{\rho_0} = g(\beta F_S - \alpha F_T) = g\beta F_S\left(1 - \frac{\alpha F_T}{\beta F_S}\right), \tag{2}$$

Then, Eq. (1) can be rewritten as

$$\varepsilon = -g\beta F_S\left(1 - \frac{\alpha F_T}{\beta F_S}\right) = -g\beta F_S\left(1 - \gamma^{\mathrm{SF}}\right), \tag{3}$$

where γ^{SF} is the density flux ratio due to SF (see Appendix B). Here, the square of buoyancy frequency N is described as

$$N^2 = -\frac{g}{\rho_0}\frac{\partial \bar{\rho}}{\partial z} = g\alpha\frac{\partial \bar{T}}{\partial z} - g\beta\frac{\partial \bar{S}}{\partial z} = -g\beta\frac{\partial \bar{S}}{\partial z}\left(1 - R_\rho\right). \tag{4}$$

From the definition of K_S and K_T in DDC (Eq. 101) with Eq. 4, we obtain an expression for the vertical eddy diffusivity of salt for SF K_S^{SF}:

$$K_S^{\mathrm{SF}} = \frac{R_\rho - 1}{1 - \gamma^{\mathrm{SF}}}\frac{\varepsilon}{N^2}. \tag{5}$$

From the definition of R_ρ, the vertical eddy diffusivity of heat for SF K_T^{SF} is given by:

$$K_T^{\mathrm{SF}} = \frac{\gamma^{\mathrm{SF}}}{R_\rho}K_S^{\mathrm{SF}} = \frac{\gamma^{\mathrm{SF}}\left(R_\rho - 1\right)}{R_\rho(1 - \gamma^{\mathrm{SF}})}\frac{\varepsilon}{N^2}. \tag{6}$$

Rewriting Eq. (82) as Eq. (7), the vertical eddy diffusivity of the density of SF K_ρ^{SF} can be written as Eq. (8):

$$-K_\rho\frac{g}{\rho_0}\frac{\partial \bar{\rho}}{\partial z} = g\alpha K_T\frac{\partial \bar{T}}{\partial z} - g\beta K_S\frac{\partial \bar{S}}{\partial z} \tag{7}$$

$$K_\rho^{\mathrm{SF}} = \frac{K_T^{\mathrm{SF}}R_\rho - K_S^{\mathrm{SF}}}{R_\rho - 1} \tag{8}$$

From Eqs. (5, 6, 7, and 8), we have

$$K_\rho^{\mathrm{SF}} = -\frac{\varepsilon}{N^2} < 0. \tag{9}$$

Eddy diffusivities for DC (K_S^{DC}, K_T^{DC}, and K_ρ^{DC}) are obtained in the same way:

$$K_S^{\mathrm{DC}} = \gamma^{\mathrm{DC}} R_\rho K_T = \frac{\gamma^{\mathrm{DC}}(1-R_\rho)}{(1-\gamma^{\mathrm{DC}})}\frac{\varepsilon}{N^2} \tag{10}$$

$$K_T^{\mathrm{DC}} = \frac{(1-R_\rho)}{R_\rho(1-\gamma^{\mathrm{DC}})}\frac{\varepsilon}{N^2}, \tag{11}$$

$$K_\rho^{\mathrm{DC}} = \frac{K_T^{DC}R_\rho - K_S^{DC}}{R_\rho - 1} = -\frac{\varepsilon}{N^2} < 0. \tag{12}$$

Note that K_ρ is negative in the presence of DDC, indicating that DDC reduces the potential energy of the system and intensifies density stratification. Using the flux laws created by Huppert (1971, Eq. 102), Kunze (1987, Eq. 93), and Kelley (1986, Eq. 94, Kelley 1990, Eq. 103), variations of the eddy diffusivity in DDC with inactive CT (taking $\varepsilon = 10^{-10}$ W kg^{-1} and $N = 5.2 \times 10^{-3}$) are shown in Fig. 1. K_S^{SF} and K_T^{SF} take large values with active SF ($1 < R_\rho < 2$).K_S^{DC} and K_T^{DC} take large values with active DC ($0.5 < R_\rho < 1$). The validity of this range will be confirmed in the next section.

3 DDC in SMC

When estimating the eddy diffusivity in the presence of DDC, the effect of velocity shear has been traditionally ignored. Linden (1974) experimentally showed that three-dimensional SF in the steady shear flow aligned with the velocity shear to form two-dimensional sheets, and with the resultant vertical transports of salt and heat remaining unchanged. However, Kunze (1990) analyzed C-SALT data and confirmed that oceanic SF should take the form of two-dimensional sheets due to velocity shear, leading to a reduction in the vertical buoyancy flux of SF. Wells et al. (2001) numerically and experimentally investigated the structure of SF in the presence of periodic shear flow, with the results revealing a reduced vertical buoyancy flux of SF. Therefore, we cannot neglect the shear effects on DDC.

For investigating the effect of shear on both DDC and CT, SMC was employed by Canuto et al. (2008), Kantha and Carniel (2009), and Kantha (2012). In this review, we follow the approach used in Kantha et al. (2011) and Kantha (2012), including the variances of both temperature and salinity in the steady-state energy equation (Eq. 79). The turbulent timescale τ is introduced as

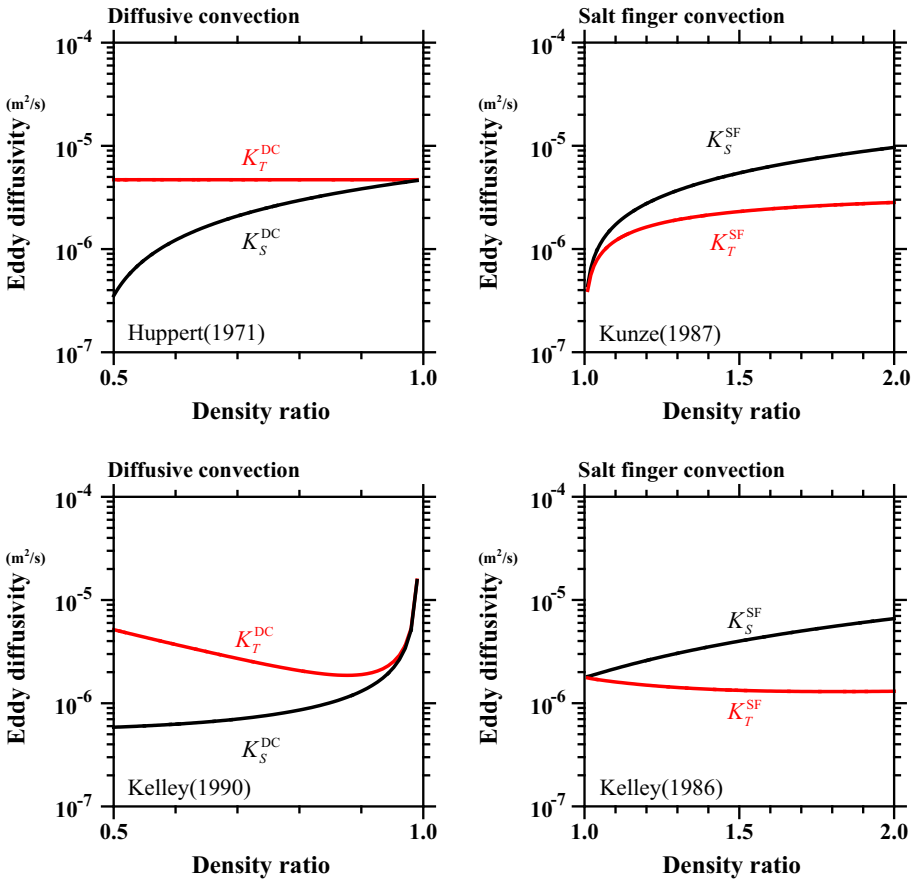

Fig. 1 Eddy diffusivities calculated from flux laws created by Huppert (1971); Kunze (1987) and Kelley (1986, 1990), taking $\varepsilon = 10^{-10}$ W kg^{-1} and $N = 5.2 \times 10^{-3}$ s^{-1} (mode values for both quantities obtained in NATRE, Gregg 1989)

$$\tau = B_1 \frac{\ell}{q} = \frac{q^2}{\varepsilon} = \frac{2K}{\varepsilon}, \tag{13}$$

where B_1 is the coefficient for the turbulent timescale, q is the turbulence velocity scale, ℓ is the turbulence length scale, and K is the TKE ($= q^2/2$). The second-moment terms of transport for heat $\overline{w'T'}$, salt $\overline{w'S'}$, and momentum $\overline{u'w'}$ are parameterized in Eqs. (80, 81 and 88) (the first-order closure), and the structure functions for the salt S_S, heat S_T, density S_ρ, and momentum S_υ are introduced with the eddy diffusivity for salt K_S, temperature K_T, density K_ρ, and momentum K_υ, defined as:

$$K_S = K\tau S_S \tag{14}$$

$$K_T = K\tau S_T \tag{15}$$

$$K_\rho = K\tau S_\rho \tag{16}$$

$$K_\upsilon = K\tau S_\upsilon \tag{17}$$

From Eq. (8) or Eq. (12), relations among S_S, S_T, and S_ρ can be obtained:

$$S_\rho = \frac{R_\rho S_T - S_S}{R_\rho - 1}. \tag{18}$$

This model is described in Appendix C. After a series of manipulations involving Eqs. (52, 71, and 72) using Eqs. (105, 106, 107, 108, 109, 110, 111, and 112), one can obtain the relations between the structure functions in the DDC as functions of the gradient Richardson number R_i, defined as Eq. (90), R_ρ and N:

$$\tau^2 N^2 \frac{R_\rho}{(R_\rho - 1)} \left[S_\upsilon \frac{(R_\rho - 1)}{R_\rho R_i} - \left(S_T - \frac{S_S}{R_\rho} \right) \right] = 2. \tag{19}$$

Introduce the non-dimensional numbers, G_T and G_υ such that

$$G_T = \tau^2 N^2, \tag{20}$$

$$G_\upsilon = \tau^2 \left(\frac{\partial \bar{u}}{\partial z} \right)^2. \tag{21}$$

Using Eqs. (20 and 21), we have the ratio between G_T and G_υ as follows

$$\frac{G_T}{G_\upsilon} = \frac{N^2}{\left(\frac{\partial \bar{u}}{\partial z} \right)^2} = R_i \tag{22}$$

Using Eq. (22), Eq. (19) can be written as

$$S_\upsilon G_\upsilon - \frac{G_T R_\rho}{(R_\rho - 1)} \left(S_T - \frac{S_S}{R_\rho} \right) = 2 \tag{23}$$

From Eqs. (13, 14, 15, 16, 17, 18, and 20), Eq. (23) becomes:

$$\frac{K_\upsilon}{R_i} - \frac{K_T R_\rho - K_S}{R_\rho - 1} = \frac{\varepsilon}{N^2}. \tag{24}$$

When shear is ignored ($R_i \gg 1$, DDC only), Eq. (23) is reduced to

$$S_S G_T - R_\rho S_T G_T = 2(R_\rho - 1). \tag{25}$$

In this case, Eq. (24) becomes equivalent to Eqs. (8 and 12). Thus, negative diffusion of density is obtained.

Kantha (2012) obtained the density flux ratio as a function of R_ρ such that

$$\gamma = \frac{R_\rho \left\{ \lambda_9 + \left[\lambda_{11} \left(\frac{1}{R_\rho} + 1 \right) - \lambda_{10} \frac{1}{R_\rho} \right] C_{\mathrm{SMC}} \right\}}{\left\{ \lambda_5 + \left[\lambda_8 - \lambda_{11} \left(\frac{1}{R_\rho} + 1 \right) \right] C_{\mathrm{SMC}} \right\}}, \tag{26}$$

and obtained relations among the structure functions for DDC without shear for SF:

$$S_T = \frac{2\gamma^{\mathrm{SF}}}{C_{\mathrm{SMC}}(1 - \gamma^{\mathrm{SF}})}, \tag{27}$$

$$S_S = \frac{R_\rho}{\gamma^{\mathrm{SF}}} S_T, \tag{28}$$

$$S_\rho = -\frac{R_\rho (1 - \gamma^{\mathrm{SF}})}{\gamma^{\mathrm{SF}} (R_\rho - 1)} S_T, \tag{29}$$

and for DC:

$$S_T = -\frac{2}{C_{\mathrm{SMC}}(1 - \gamma^{\mathrm{DC}})}, \tag{30}$$

$$S_S = R_\rho \gamma^{\mathrm{DC}} S_T, \tag{31}$$

$$S_\rho = -\frac{R_\rho (1 - \gamma^{\mathrm{DC}})}{1 - R_\rho} S_T. \tag{32}$$

C_{SMC} is a parameter to be determined. Here, we have used γ obtained by Kelley (1986, Eq. 94 for SF and Eq. 103 for DC) on the left-hand side of Eq. 26 to calculate C_{SMC}, and then to calculate the structure functions (Eqs. 27, 28, 29, 30, 31, 32, Fig. 2). S_S and S_T steeply increased as R_ρ approached unity, which means that mixing due to DDC was intensified. Negative S_ρ for both SF and DC implies negative diffusion of density. These functions indicate that the effect of DDC is certainly important but is restricted to a narrow range of R_ρ ($0.8 \sim 1.2$). This point should be investigated in greater detail in future modeling studies.

SMC theories continue to be developed; however, there is difficulty when it comes to observational usage. Therefore, other parameterizations, which are mentioned in Sects. 3 and 4, have been proposed.

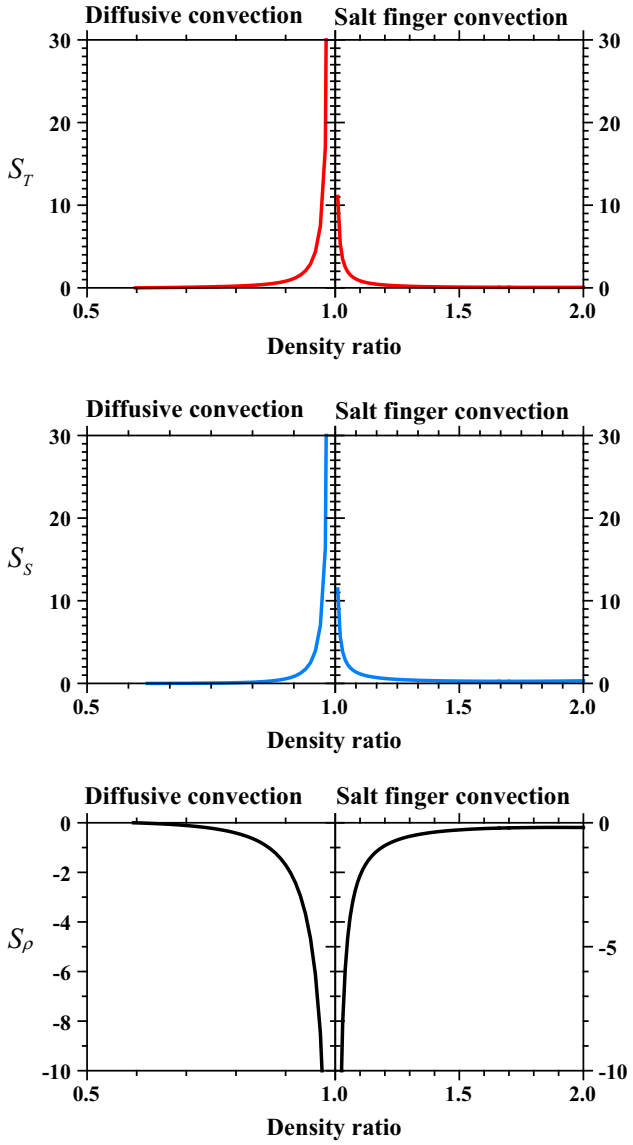

Fig. 2 Dependence of structure functions for (top) heat S_T, (middle) salt S_S, and (bottom) density S_ρ on R_ρ

4 K-profile parameterization with DDC

Large et al. (1994) simulated meridional ocean circulation (MOC) using K-profile parameterization (KPP) and considered three different mechanisms that contribute to eddy diffusivity, namely vertical shear instability, IW breaking, and DDC, providing a linear combination for eddy diffusivity: $K_\rho = K_\rho^{\mathrm{Shear}} + K_\rho^{\mathrm{IW}} + K_\rho^{\mathrm{DDC}}$. When active SF occurred ($1 < R_\rho < 1.9$), they used a constant value of 0.7 for γ^{SF}, describing K_S^{SF} and K_T^{SF} as

$$K_S^{\mathrm{SF}} = \left[1 - \left(\frac{R_\rho - 1}{0.9}\right)^2\right]^3 \times 10^{-3}, \tag{33}$$

$$K_T^{\mathrm{SF}} = \frac{\gamma^{\mathrm{SF}}}{R_\rho} K_S^{\mathrm{SF}}. \tag{34}$$

When R_ρ was greater than 1.9, $K_S^{\mathrm{SF}} = 0$. In the case of active DC ($0.5 < R_\rho < 1$), K_T^{DC} is calculated using γ^{DC} as proposed by Marmorino and Caldwell (1976) and K_S^{DC} as proposed by Huppert (1971, Eq. 102):

$$K_T^{\mathrm{DC}} = 0.909 \times 1.5 \times 10^{-6} \exp\left[4.6 \exp\left(-0.54\left(R_\rho^{-1} - 1\right)\right)\right], \tag{35}$$

$$K_S^{\mathrm{DC}} = (1.85 - 0.85 R_\rho^{-1}) R_\rho K_T^{\mathrm{DC}}. \tag{36}$$

If R_ρ was less than 0.5,

$$K_S^{\mathrm{DC}} = 0.15 R_\rho K_T^{\mathrm{DC}}. \tag{37}$$

Zhang et al. (1998) also simulated the MOC using a parameterization considering DDC effects. They defined the background diffusivity as $K_b = 3 \times 10^{-5}$ m^2/s and parameterized SF and DC eddy diffusivity. When SF occurred, they used a constant value of 0.7 for γ^{SF} and described K_S^{SF} and K_T^{SF} as

$$K_S^{\mathrm{SF}} = \frac{1 \times 10^{-4}}{1 + \left(\frac{R_\rho}{1.6}\right)^6} + K_b, \tag{38}$$

$$K_T^{\mathrm{SF}} = \frac{\gamma^{\mathrm{SF}}}{R_\rho}\left(K_S^{\mathrm{SF}} - K_b\right) + K_b. \tag{39}$$

When DC occurred, they used the γ^{DC} presented by Kelley (1984), wherein the molecular heat diffusivity $k_T = 1.5 \times 10^{-7}$ m^2 s^{-1}, and they described K_S^{DC} and K_T^{DC} as

$$K_S^{\mathrm{DC}} = R_\rho \gamma^{\mathrm{DC}} (K_T^{\mathrm{DC}} - K_b) + K_b, \tag{40}$$

$$K_T^{\mathrm{DC}} = 0.0032 \exp\left(4.8 R_\rho^{0.72}\right) \cdot \left(0.25 \times 10^9 R_\rho^{-1.1}\right)^{1/3} \cdot k_T + K_b. \tag{41}$$

For both treatments, K_ρ^{DDC} is taken as

$$K_\rho^{\mathrm{DDC}} = \frac{K_T^{\mathrm{DDC}} R_\rho - K_S^{\mathrm{DDC}}}{R_\rho - 1}. \tag{42}$$

A calculation of the eddy diffusivities in the range of $0.5 < R_\rho < 2$ is shown in Fig. 3.

The parameterization set by Zhang et al. (1998) has smaller values than that of Large et al. (1994). However, the absolute diffusivity values in both parameterizations increase as R_ρ approaches unity. When R_ρ becomes smaller than 1.7, K_ρ^{SF} becomes negative. The notable difference between Zhang et al. (1998) and Large et al. (1994) is the behavior around $R_\rho = 1$. Both K_ρ^{SF} diverge negatively, but Large et al. (1994)'s K_ρ^{SF} rapidly diverges because of the relatively large differences between K_S^{SF} and K_T^{SF}. As for

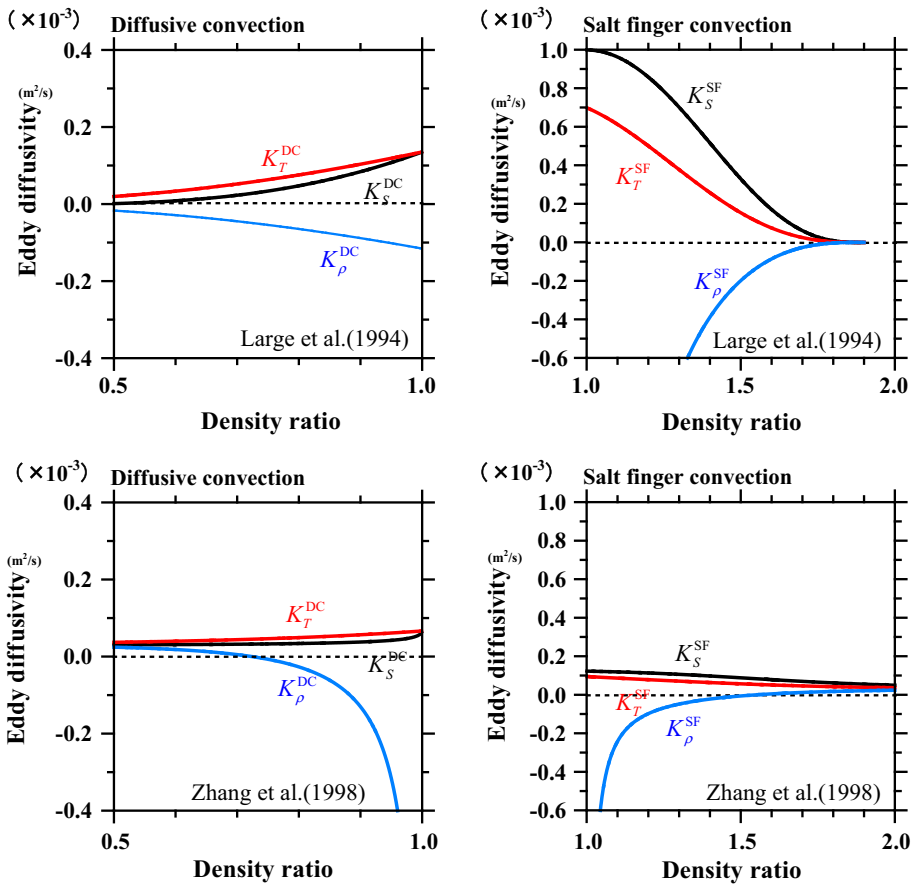

Fig. 3 Eddy diffusivities employed for numerical simulations by Large et al. (1994) and Zhang et al. (1998)

K_ρ^{DC}, when we take the limit of K_ρ^{DC} as R_ρ approaches unity, K_ρ^{DC} diverges negatively for Zhang et al. (1998) while becoming nearly constant for Large et al. (1994).

Merryfield et al. (1999) used parameterization similar to that of Zhang et al. (1998), which changed the background diffusivity. Following studies by following Gargett (1984) and Gargett and Holloway (1984), they defined the background diffusivity as proportional to N^{-1}, and found that relatively minor changes occurred in the global circulation (mass transport) even when DDC was present. Nevertheless, there were substantial changes in the local temperature and salt distributions: the lower layer became saltier because of the efficient salt transport resulting from SF. Inoue et al. (2007) analyzed turbulence data observed in a perturbed region off Sanriku Coast, Japan, and compared their observed diffusivity values with those of Zhang et al. (1998, Eqs. 38, 39, and 40). This comparison showed a fairly good agreement for SF, but not for DC.

5 Direct numerical simulation of DDC

Recent developments in computer power have enabled us to conduct DNS of DDC. Such studies have the advantage of directly estimating the vertical fluxes and diffusivities. Kimura et al. (2011) conducted DNS at low R_ρ (< 2.0, active SF). The study showed that when SF develops, both K_S^{SF} and K_T^{SF} increase as R_i increases, which is an unexpected result. In typical cases, a shear instability (energy source) should be inactive as R_i increases, with both K_S^{SF} and K_T^{SF} increasing as R_ρ decreases. This result agrees with previous theoretical, observational, and situational estimations. The result follows the functional dependency of diffusivity on R_i and R_ρ:

$$K_S^{\mathrm{SF}} = 4.38 \times 10^{-5} R_\rho^{-2.7} R_i^{0.17}, \tag{43}$$

$$K_T^{\mathrm{SF}} = 3.07 \times 10^{-5} R_\rho^{-4.0} R_i^{0.17}. \tag{44}$$

This parameterization was verified and improved by Nakano et al. (2014), who analyzed the microstructure and CTD/LADCP results in the perturbed region off the Sanriku Coast, Japan, and western North Pacific Ocean. They also employed the buoyancy Reynolds number R_{eb} and R_i (both at 10 m scale) as the distinguishing parameters

between CT and DDC. They obtained the following new relationship between R_{eb} and R_i:

$$R_{eb} = 19.5R_i^{-1.03}. \tag{45}$$

From this relation, we can obtain critical values for R_{eb} from R_i such that:

$$(R_{eb}, R_i)=(80, 0.25), (20, 1).$$

The value of R_i = 1 is the stability criterion of the water column, and if $R_i < 0.25$, the water column can become unstable and turbulent. Therefore, values of R_{eb}= 20 and 80 corresponding to R_i, which indicate that $R_{eb}< 80$ and $R_i> 0.25$, are suitable as criteria for the onset of DDC. Taking into account this criteria, Nakano et al. (2014) applied a DNS parameterization of diffusivity as the functions of R_i and R_ρ (Kimura et al. 2011, Eqs. 43 and 44), improving their functional dependency using the following equations:

$$\left.\begin{aligned} K_S^{\mathrm{SF}} &= 9.35 \times 10^{-5} R_\rho^{-2.7} R_i^{0.17} \\ K_T^{\mathrm{SF}} &= 7.61 \times 10^{-5} R_\rho^{-2.7} R_i^{0.17} \end{aligned}\right\}, R_i > 0.25 (R_{eb} < 80). \tag{46}$$

The estimated average diffusivities of salt and heat are 2.2×10^{-5} m^2/s and 3.5×10^{-5} m^2/s (R_ρ= 1.25), and 3.5×10^{-5} m^2/s and 1.1×10^{-4} m^2/s (R_ρ= 1.75), respectively. It was considered that the difference in coefficients between DNS (Eqs. 43, 44) and observation (Eq. 46) was caused by vertical scale difference.

Radko and Smith (2012) conducted fine-grid simulations and non-dimensional analyses of typical SF width and length scales at R_ρ= 1.9. They produced vertically aligned fingers disturbed by a secondary instability. In their calculations, fluxes become almost constant after a secondary instability became comparable to the elevator mode. They obtained γ as a function of R_ρ, which agrees fairly well with the laboratory prediction:

$$F_S^{\mathrm{SF}} = \frac{135.7}{\sqrt{R_\rho - 1}} - 62.75, \tag{47}$$

$$\gamma^{\mathrm{SF}} = 2.709 \exp\left(-2.513 R_\rho\right) + 0.5128, \tag{48}$$

$$F_T^{\mathrm{SF}} = \gamma^{\mathrm{SF}} F_S^{\mathrm{SF}}. \tag{49}$$

As mentioned above, although parameterizations will continue to be refined with increasing computer machine power, verification of parameterization with observational data is still required.

6 Key points of eddy diffusivity estimation with measurement data

6.1 Mixing coefficients and distinguishing DDC from CT

Most microstructure observations aimed at evaluating eddy diffusivity in the presence of DDC have been based on observations of the dissipation rate of temperature variance χ_T (and thus, K_T estimation by Eq. 86) and mixing efficiency Γ.

To elucidate the effects of microstructures, eddy diffusivity of density for CT generated by shear K_ρ^{CT} is parameterized as follows:

$$K_\rho^{\mathrm{CT}} = \Gamma^{\mathrm{CT}} \frac{\varepsilon}{N^2}, \tag{50}$$

where Γ^{CT} is the mixing coefficient for CT, which can be regarded as the mixing efficiency. A detailed derivation of Eq. (50) is presented in Appendix A. Γ^{CT} is the result of the observed values of ε, χ_T, density stratification, and temperature stratification (see Eq. 86), but Γ^{CT} has been considered to have a constant value of 0.2 or 0.25 (e.g., Osborn 1980; Oakey 1982). Thus, K_ρ^{CT} is calculated using ε and N. However, the results discussed in the previous studies cast doubt on the validity of using a constant value for Γ^{CT} (= 0.2) when estimating the eddy diffusivity in the presence of DDC.

When estimating eddy diffusivity in the presence of DDC, non-dimensional parameters, such as R_ρ, and R_i measured by the vertical velocity shear $\frac{\partial \overline{u}}{\partial z}$, N and R_{eb} (see Eq. 92) have been used to distinguish between CT and DDC. Also, the value of Γ for DDC (Γ^{DDC}) is a key factor in distinguishing DDC from CT. The definition of Γ^{DDC} is the same as Γ^{CT} via observation (right-hand side of Eq. 86):

$$\Gamma^{\mathrm{DDC}} = \frac{\chi_T N^2}{2\varepsilon \left(\frac{\partial \overline{T}}{\partial z}\right)^2}. \tag{51}$$

Historically, Γ^{DDC} has been investigated separately from SF (Γ^{SF}) or DC (Γ^{DC}). St. Laurent and Schmitt (1999) surveyed the distributions of Γ^{SF} and Γ^{DC} with R_ρ and R_i and found that Γ^{SF} and Γ^{DC} increased substantially because of DDC. This is one of the current key issues in microstructure studies (e.g., de Lavergne et al. 2016). This is readily understood because DDC can efficiently diffuse temperature fluctuations and create a large diffusion of temperature (Fig. 4). Inoue et al. (2007) proposed that DDC is effective in mixing when $R_{eb}< 20$ in the perturbed region. Inoue et al. (2008) revisited North Atlantic Tracer Release Experiment (NATRE) data, adding the R_i criterion to restrict their attention to cases when CT was not active

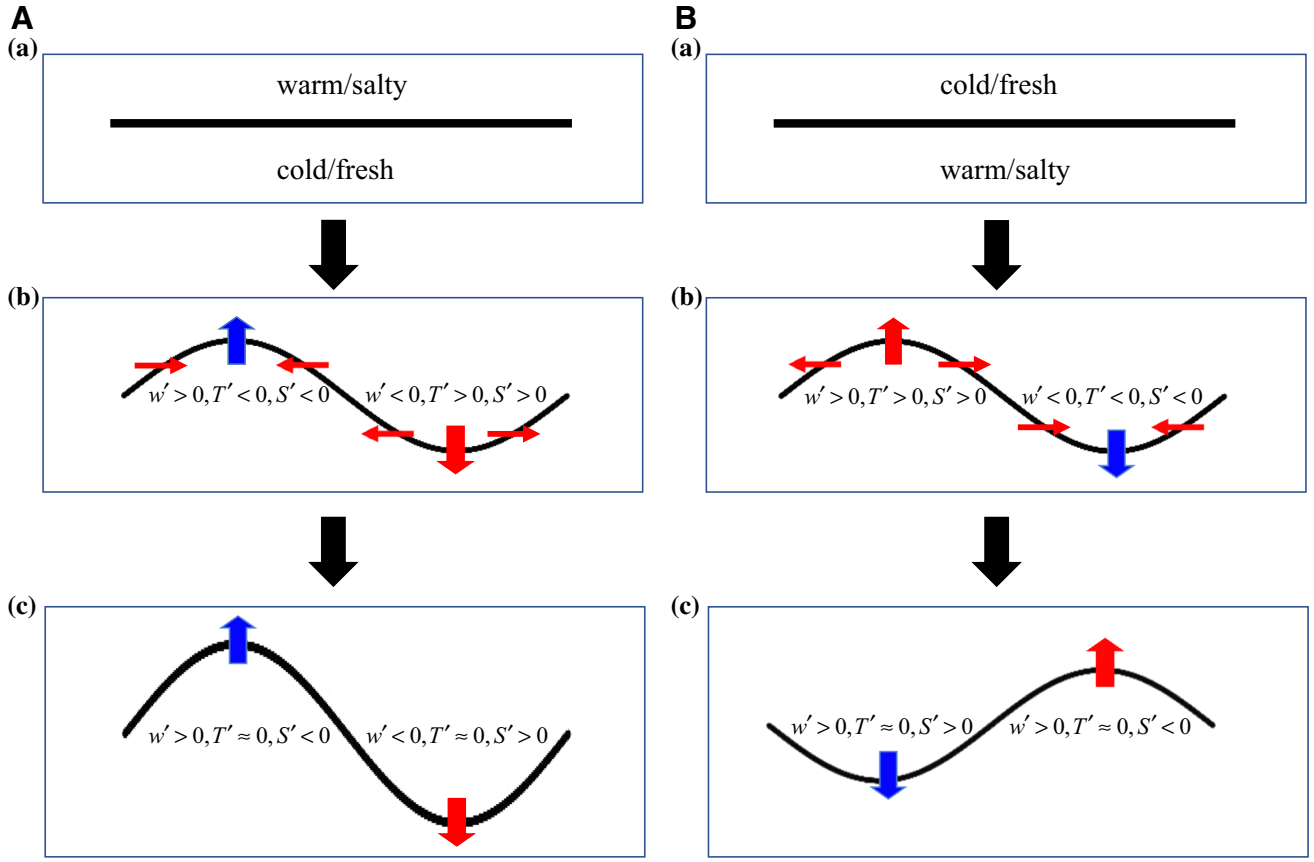

Fig. 4 **a** Occurrence of diffusive convection. (a) Initially warm/salty layer is above, and the cold/fresh layer is below. The separating interface is initially at rest. (b) The interface becomes unstable because of differences in molecular diffusivity of heat and salt ($k_T \approx 100 k_S$). The upward portion of the lower layer ($w' > 0$, vertical blue arrow) has both negative temperature and salt anomalies due to a surrounding warm and salty layer ($T' < 0$ and $S' < 0$). The downward portion ($w' < 0$, vertical red arrow) has positive temperature and salt anomalies due to a surrounding cold fresh layer ($T' > 0$ and $S' > 0$). Lateral molecular diffusion of heat is greater than that of salt. Therefore, the upward portion is warmed and the downward portion is cooled. (c) Consequently, the upward portion attains a positive buoyancy force and keeps ascending upward (vertical blue arrow), whereas the downward portion attains a negative buoyancy force, causing its descent downward (vertical red arrow). The motions are aligned horizontally to form a salt finger cell. **b** Occurrence of diffusive convection. (a) Initially, cold/fresh layer is above, and the warm/salty layer is below. The separating interface is initially at rest. (b) The interface becomes unstable to be wavy because of differences in molecular diffusivity of heat and salt ($k_T \approx 100\ k_S$). The upward portion from the lower layer ($w' > 0$, vertical red arrow) has positive temperature and salt anomalies from a surrounding cold and fresh layer ($T' > 0$ and $S' > 0$). The negative portion from the lower layer ($w' < 0$, vertical blue arrow) has negative temperature and salt anomalies from a surrounding warm and salty layer ($T' > 0$ and $S' > 0$). Lateral molecular diffusion of heat is greater than that of salt. Therefore, the upward portion is cooled and the downward portion is warmed. (c) Consequently, the upward portion receives negative buoyancy force and descends downward (vertical blue arrow), whereas the downward portion obtains positive buoyancy force and ascends upward (vertical red arrow). These upward and downward portions lose or gain heat repeatedly from the surrounding water. These upward and downward motions repeat to produce mixed layers separated by the interface to form a clear diffusive interface

($R_i > 0.25$ and $R_{eb} < 20$). They found that Γ^{SF} decreased when R_ρ increased:

$$\left(\Gamma^{\mathrm{SF}}, R_\rho\right) = (1.0, 1.3), (0.6, 1.9),$$
$$\left(\Gamma^{\mathrm{SF}}, R_i\right) = (0.6, 0.4), (0.9, 1.0), (1.3, 10).$$

Nakano (2016) analyzed the TurboMAP and CTD/LADCP data at 10 m scale and surveyed Γ^{DDC} for wide ranges in R_i and R_{eb} values, showing that Γ^{DDC} became large as R_i increased and R_{eb} decreased (Fig. 5, also see Eq. 45). Large values of Γ^{DDC} apparently stem from the large values of χ_T (Eq. 75) in DDC. Previous investigations cited above also showed low ε and high χ_T values in DDC layers, resulting in large values of Γ^{DDC}. The observed values of Γ are summarized in Table 1. Taken together, it is certain that Γ^{DDC} takes a large value. Thus, in evaluating the eddy diffusivity in the presence of DDC, the use of Γ^{CT} (~ 0.2) should be avoided.

6.2 Practical eddy diffusivity estimation

St. Laurent and Schmitt (1999) calculated K_T (as shown in Table 2 together with other estimations). They separated

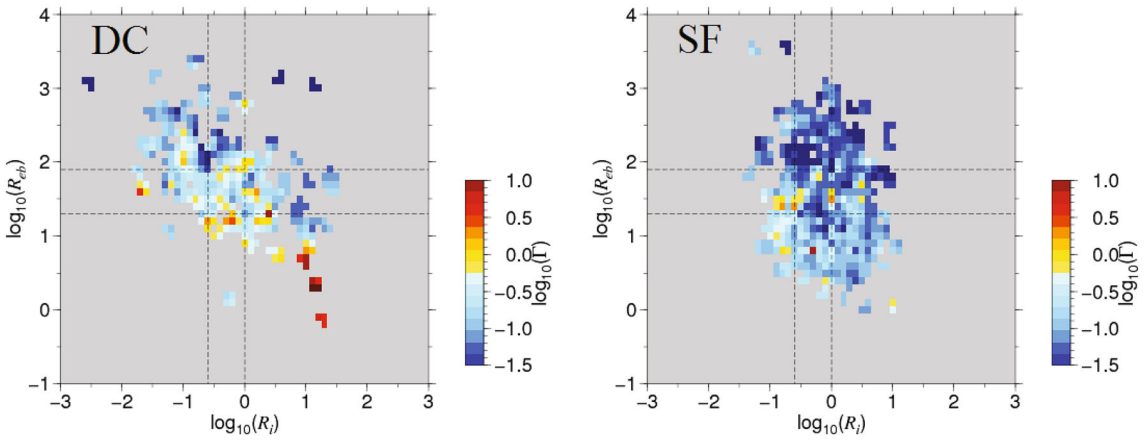

Fig. 5 Γ plots on Log(R_{eb}) − Log(R_i) plane. Data were obtained from the western North Pacific Ocean (Nakano et al. 2014)

Table 1 Examples of direct estimation of Γ in the presence of DDC

References	Location	Microstructure instrument	Resolution of microstructure data (m)	SF or DC	R_ρ	Other limitations	Γ
Oakey (1988)	Atlantic Ocean, Meddy	EPSONDE	1.5–2	SF	unknown	–	> 1
				DC			
St. Laurent and Schmitt (1999)	NATRE	HRP	5	SF	∼ 2	$1 < R_i < 100$ (not turbulent)	> 0.6
Inoue et al. (2007)	Perturbed region off the Sanriku Coast, Japan	TurboMAP	2	SF	1–3	–	0.46
				DC	1/3–1		1.20
Inoue et al. (2008)	NATRE	HRP	10	SF	1.3	–	1.0
				SF	1.9		0.6
Ishizu et al. (2012)	Soya Current	TurboMAP	1	DC	unknown	–	>1
Nakano et al. (2014)	Western North Pacific Ocean	TurboMAP with CTD + LADCP	10	SF	1–5	–	0.3
				DC	0.5–1		10
Nagai et al. (2015)	Kuroshio Extension	MicroRider	1.7-4.2	SF	$45° < Tu < 90°$	–	1.2
		EM-APEX		DC	$90° < Tu < 45°$		4.0

EPSONDE Epsilon SONDE, *HRP* high-resolution profiler, *TurboMAP* turbulence ocean microstructure acquisition profiler, *EM-APEX* electromagnetic autonomous profiling explorer, *NATRE* North Atlantic Tracer Release Experiment

the observed layers as favorable to either DDC or CT in order to calculate the percentages of DDC and CT layers. In addition, they obtained weighted averages of diffusivities at almost 100 m depth intervals. Relatively high values ($\sim 10^{-4}$ m^2/s) were obtained at 90 m depth, but values were generally lower below the thermocline. Inoue et al. (2007) presented four scenarios for estimating diffusivity and vertical buoyancy flux: (1) CT (2), DDC, (3) a simple average of CT and DDC, and (4) weighted average of CT and DDC. They concluded that scenario (4) provided the best estimation for diffusivity due to DDC and CT (1.56×10^{-5} m^2/s for heat, 1.85×10^{-5} m^2/s for salt). Nakano et al. (2014) also obtained a relatively small diffusivity value (10^{-5} m^2 /s). Schmitt et al. (2005) estimated a relatively high diffusivity value for salt ($> 10^{-4}$ m^2/s) in the western Tropical Atlantic Ocean using Eq. (5). Ishizu et al. (2012) and Nagai et al. (2015) obtained a high diffusivity value ($> 10^{-4}$ m^2/s) under the Soya Current and the Kuroshio Extension, respectively.

7 Concluding remarks

In oceanic regions susceptible to DDC, parameterizations of K_S^{DDC} and K_T^{DDC} have been carried out under the assumption that velocity shear is negligible. However, CT

Table 2 Examples of direct estimation of eddy diffusivity in the presence of DDC

References	Location	Microstructure instrument	SF or DC and	Observed parameters	Diffusivity
St. Laurent and Schmitt (1999)	NATRE	HRP	SF (R_ρ= 1.5–2.0)	ε, R_ρ, χ_T, R_i	K_T: 0.08 × 10^{-4} m^2/s K_S: 0.13 × 10^{-4} m^2/s
Schmitt et al. (2005)	Western Tropical Atlantic Ocean	HRP	SF (R_ρ= 1.71)	ε, R_ρ, χ_T	K_T: 1.07 × 10^{-4} m^2/s K_S: 2.40 × 10^{-4} m^2/s
Inoue et al. (2007)	Perturbed region off the Sanriku Coast, Japan	TurboMAP	SF (R_ρ= 1–3) DC (R_ρ= 1/3–1)	ε, R_ρ, χ_T	K_T: 1.56 × 10^{-5} m^2/s K_S: 1.85 × 10^{-5} m^2/s
Ishizu et al. (2012)	Soya Current	TurboMAP	DC (R_ρ: unknown)	ε, R_ρ, χ_T	$K_{T,S}$: > 10^{-4} m^2/s
Nakano et al. (2014)	Western North Pacific Ocean	TurboMAP with CTD + LADCP	SF (R_ρ= 1.25–1.75)	ε, R_ρ, R_{eb}	K_T: (2.2–3.5) × 10^{-5} m^2/s K_S: (3.5–11) × 10^{-5} m^2/s
Nagai et al. (2015)	Kuroshio Extension	MicroRider EM-APEX	SF (R_ρ> 1) DC ($0 < R_\rho < 1$)	ε, R_ρ, χ_T,R_{eb}	K_T: $O(10^{-3}$ $m^2/s)$

HRP high-resolution profiler, *TurboMAP* turbulence ocean microstructure acquisition profiler

is a common feature in the Global Ocean and can coexist with DDC. Therefore, in this note, parameterizations of DDC in oceanic mixing processes are reviewed and their applicability assessed.

The notion of representing DDC in TKE with an inactive CT variable was introduced. The applicability of DDC was investigated using an SMC model. In cases where DDC and CT coexist, the effect of DDC is certainly important but is restricted to a narrow range of R_ρ (0.8–1.2). Some DDC parameterizations used in numerical simulations were reviewed in terms of physical empirical validity and applicability. An approximation can be made by combining R_ρ and R_i to roughly estimate the eddy diffusivity for SF, but these parameterizations are currently being verified. A mixing coefficient is required to distinguish DDC from CT and is related to R_ρ and R_i. The details of this relationship require further scientific study.

Therefore, measurements of R_i, R_{eb}, and R_ρ are essential for determining the intensity of mixing due to DDC. When measuring the eddy diffusivity in the ocean interior, it is thus necessary to deploy an ADCP/LADCP or electromagnetic current meter, along with a microstructure profiler. The accumulation of observations gained by these instruments will improve the ability to map eddy diffusivity in the Global Ocean, potentially leading to better parameterization of eddy diffusivity in numerical modeling.

Acknowledgements This work is part of Haruka Nakano's PhD thesis (Nakano 2016). The manuscript was prepared under the guidance of Prof. Kantha (University of Colorado). The work is supported by MEXT KAKENHI grant number JPH05817.

Appendix A Parameterization of eddy diffusivity in a turbulent, non-double-diffusive system

A.1 TKE equation

To parameterize eddy diffusivity in a CT system without DDC, we use the TKE equation derived from the momentum equation (e.g., Kantha 2012), as follows:

$$\bar{\rho}\frac{\partial}{\partial t}\left(\frac{1}{2}\overline{u_i'u_i'}\right)+\bar{\rho}\bar{u}_j\frac{\partial}{\partial x_j}\left(\frac{1}{2}\overline{u_i'u_i'}\right)$$
$$=-\frac{\partial}{\partial x_j}\left(\overline{p'u_j'}+\frac{1}{2}\bar{\rho}\overline{u_i'u_i'u_j'}-\bar{\rho}\upsilon\frac{\partial}{\partial x_j}\left(\overline{u_i'\left(\frac{\partial u_i'}{\partial x_j}+\frac{\partial u_j'}{\partial x_i}\right)}\right)\right)$$
$$-\frac{1}{2}\bar{\rho}\overline{u_i'u_j'}\left(\frac{\partial\bar{u}_i}{\partial x_j}+\frac{\partial\bar{u}_j}{\partial x_i}\right)-\overline{u_i'\rho'g\delta_{i3}}-\frac{\bar{\rho}\upsilon}{2}\overline{\left(\frac{\partial u_i'}{\partial x_j}+\frac{\partial u_j'}{\partial x_i}\right)^2}, \tag{52}$$

$$\frac{d}{dt}\left(\frac{1}{2}\overline{u_i'u_i'}\right)=-\frac{\partial}{\partial x_j}\left(D_{ij}\right)-\frac{1}{2}\overline{u_i'u_j'}\left(\frac{\partial\bar{u}_i}{\partial x_j}+\frac{\partial\bar{u}_j}{\partial x_i}\right)$$
$$-\frac{\overline{u_i'\rho'g\delta_{i3}}}{\bar{\rho}}-\frac{1}{2}\upsilon\overline{\left(\frac{\partial u_i'}{\partial x_j}+\frac{\partial u_j'}{\partial x_i}\right)^2} \tag{53}$$

Here, variables (u: velocity, p: pressure, T: temperature, S: salinity and ρ: density) are divided into mean and fluctuation (turbulence) components as $u_i=\bar{u}_i+u_i'$, $p=\bar{p}+p'$, $T=\bar{T}+T'$, $S=\bar{S}+S'$, and $\rho=\bar{\rho}+\rho'$. Indices (i, j) take the values 1, 2, and 3, which correspond to the x-, y-, and z-direction; g is the gravitational acceleration. Einstein's law of summation is applied, in which a summation is made over three values repeated in the expression for the general term (Hinze 1975, p. 774). δ_{ij} is the Kronecker delta. Overbars denote the ensemble averages. υ is the kinematic molecular viscosity ($\sim 1.05\times10^{-6}$ m^2/s at 20 °C and 34 PSU). Note that υ varies with temperature and salinity. The TKE K (in the blanket on the left-hand side of Eq. 53) is

$$K=\frac{1}{2}q^2=\frac{1}{2}\left(\overline{u'^2}+\overline{v'^2}+\overline{w'^2}\right), \tag{54}$$

where q is the turbulence velocity scale, and u', v', and w' are x, y, and z components of turbulence velocity (fluctuation components in Eq. 53).

Here, D_{ij} indicates the energy transport via the fluctuation components. $\overline{p'u_j'}$ is due to the correlation between pressure and velocity fluctuation. $\frac{1}{2}\bar{\rho}\overline{u_i'u_i'u_j'}$ is produced by the triple correlation of the velocity fluctuation. $-\bar{\rho}\upsilon\frac{\partial}{\partial x_j}\left(\overline{u_i'\left(\frac{\partial u_i'}{\partial x_j}+\frac{\partial u_j'}{\partial x_i}\right)}\right)$ is viscous dissipation. The term $-\frac{\partial}{\partial x_j}\left(D_{ij}\right)$ represents the diffusion of energy transport; this is considered to be small and is traditionally neglected.

Considering the isotropy of turbulence in three dimensions, mean velocity (also called the background velocity) in the x-direction $\bar{u}$, and its vertical variation, components of the second term on the right-hand side in Eq. (53) are described as

$$i\neq j:-\frac{1}{2}\left\{\overline{u'v'}\left(\cancel{\frac{\partial\bar{u}}{\partial y}}+\cancel{\frac{\partial\bar{v}}{\partial x}}\right)+\overline{u'w'}\left(\frac{\partial\bar{u}}{\partial z}+\cancel{\frac{\partial\bar{w}}{\partial x}}\right)\right\}$$
$$-\frac{1}{2}\left\{\overline{v'u'}\left(\cancel{\frac{\partial\bar{v}}{\partial x}}+\cancel{\frac{\partial\bar{u}}{\partial y}}\right)+\overline{v'w'}\left(\cancel{\frac{\partial\bar{v}}{\partial z}}+\cancel{\frac{\partial\bar{w}}{\partial y}}\right)\right\}$$
$$-\frac{1}{2}\left\{\overline{w'u'}\left(\cancel{\frac{\partial\bar{w}}{\partial x}}+\frac{\partial\bar{u}}{\partial z}\right)+\overline{w'v'}\left(\cancel{\frac{\partial\bar{w}}{\partial y}}+\cancel{\frac{\partial\bar{v}}{\partial z}}\right)\right\}, \tag{55}$$

$$i=j:-\frac{1}{2}\left\{\overline{u'u'}\left(2\cancel{\frac{\partial\bar{u}}{\partial x}}\right)+\overline{v'v'}\left(2\cancel{\frac{\partial\bar{v}}{\partial y}}\right)+\overline{w'w'}\left(2\cancel{\frac{\partial\bar{w}}{\partial z}}\right)\right\}. \tag{56}$$

Therefore, the second term on the right-hand side of Eq. (53) is

$$-\frac{1}{2}\overline{u_i'u_j'}\left(\frac{\partial\bar{u}_i}{\partial x_j}+\frac{\partial\bar{u}_j}{\partial x_i}\right)=-\overline{u'w'}\frac{\partial\bar{u}}{\partial z}=P. \tag{57}$$

The third term on the right-hand side of Eq. (53) is

$$-\frac{\overline{u_i'\rho'g\delta_{i3}}}{\bar{\rho}}=-\frac{\overline{\rho'w'}}{\bar{\rho}}g\ =-J_b\quad(i=3). \tag{58}$$

.

The details of the fourth term on the right-hand side of Eq. (53) are described as

$$i\neq j:-\frac{1}{2}\upsilon\left[\overline{\left(\frac{\partial u'}{\partial y}+\frac{\partial v'}{\partial x}\right)^2}+\overline{\left(\frac{\partial v'}{\partial z}+\frac{\partial w'}{\partial y}\right)^2}+\overline{\left(\frac{\partial w'}{\partial x}+\frac{\partial u'}{\partial z}\right)^2}\right]$$
$$=-\frac{1}{2}\upsilon\left[\overline{\left(\frac{\partial u'}{\partial y}\right)^2}+\overline{\left(\frac{\partial v'}{\partial x}\right)^2}+\overline{\left(\frac{\partial v'}{\partial z}\right)^2}+\overline{\left(\frac{\partial w'}{\partial y}\right)^2}\right.$$
$$+\overline{\left(\frac{\partial w'}{\partial z}\right)^2}+\overline{\left(\frac{\partial u'}{\partial z}\right)^2}+2\overline{\left(\frac{\partial u'}{\partial y}\cdot\frac{\partial v'}{\partial x}\right)}$$
$$\left.+2\overline{\left(\frac{\partial v'}{\partial z}\cdot\frac{\partial w'}{\partial y}\right)}+2\overline{\left(\frac{\partial w'}{\partial x}\cdot\frac{\partial u'}{\partial z}\right)}\right] \tag{59}$$

$$i=j:-\frac{1}{2}\upsilon\left[4\left\{\overline{\left(\frac{\partial u'}{\partial x}\right)^2}+\overline{\left(\frac{\partial v'}{\partial y}\right)^2}+\overline{\left(\frac{\partial w'}{\partial z}\right)^2}\right\}\right] \tag{60}$$

Assuming the isotropic turbulence (e.g., Yih 1979, Eqs. 61, 62 and 63), we obtain Eq. (64).

$$\overline{\left(\frac{\partial u'}{\partial x}\right)^2}=\overline{\left(\frac{\partial v'}{\partial y}\right)^2}=\overline{\left(\frac{\partial w'}{\partial z}\right)^2}=\frac{1}{2}\overline{\left(\frac{\partial u'}{\partial z}\right)^2} \tag{61}$$

$$\overline{\left(\frac{\partial u'}{\partial y}\right)^2} = \overline{\left(\frac{\partial u'}{\partial z}\right)^2} = \overline{\left(\frac{\partial v'}{\partial x}\right)^2} = \overline{\left(\frac{\partial v'}{\partial z}\right)^2} = \overline{\left(\frac{\partial w'}{\partial x}\right)^2} = \overline{\left(\frac{\partial w'}{\partial y}\right)^2} \tag{62}$$

$$\overline{\left(\frac{\partial u'}{\partial y}\cdot\frac{\partial v'}{\partial x}\right)} = \overline{\left(\frac{\partial v'}{\partial z}\cdot\frac{\partial w'}{\partial y}\right)} = \overline{\left(\frac{\partial w'}{\partial x}\cdot\frac{\partial u'}{\partial z}\right)} = \frac{1}{2}\overline{\left(\frac{\partial u'}{\partial z}\right)^2} \tag{63}$$

$$-\frac{1}{2}\upsilon\overline{\left(\frac{\partial u_i'}{\partial x_j}+\frac{\partial u_j'}{\partial x_i}\right)^2} = -\frac{15}{2}\upsilon\overline{\left(\frac{\partial u'}{\partial z}\right)^2} = -\varepsilon \tag{64}$$

Therefore, we can sum Eqs. (54, 57, 58, and 64) into Eq. (65).

$$\frac{dK}{dt} = -\overline{u'w'}\frac{\partial \bar{u}}{\partial z} - g\frac{\overline{\rho'w'}}{\bar{\rho}} - \varepsilon = P - J_b - \varepsilon, \tag{65}$$

The z-axis is taken to be positive upward. The left term of Eq. (65) is the time variation of TKE (K). The term P is the energy production of the Reynolds stress $\overline{u'w'}$ against background velocity shear ($\frac{\partial \bar{u}}{\partial z}$). $\overline{u'w'}$ is the turbulence momentum transport created by the correlation (via eddy motion) between u' and w'. It is negative if $\frac{\partial \bar{u}}{\partial z} > 0$, and positive if $\frac{\partial \bar{u}}{\partial z} < 0$. Thus, the term P is always positive, and acts as a source of TKE. The term J_b is the energy production or dissipation by the turbulent density flux $\overline{\rho'w'}$, which is created by the correlation (and also by the eddy motion) between ρ' and w'. If the density stratification is stable, $\overline{\rho'w'}$ is positive and the term J_b acts as a sink for TKE. If the density stratification is unstable, $\overline{\rho'w'}$ is negative and acts as a source for TKE. The last term ε is the TKE dissipation rate defined from the isotropic turbulence and is presented as follows (e.g., Osborn 1980):

$$\varepsilon = \frac{15}{2}\upsilon\overline{\left(\frac{\partial \bar{u}}{\partial z}\right)^2} \tag{66}$$

$\overline{\left(\frac{\partial u'}{\partial z}\right)^2}$ is the variance of turbulent velocity shear. If the turbulent field is not isotropic, $\varepsilon = \frac{15}{4}\upsilon\left[\overline{\left(\frac{\partial u'}{\partial z}\right)^2} + \overline{\left(\frac{\partial v'}{\partial z}\right)^2}\right]$ is defined as the dissipation rate (e.g., Lozovatsky and Fernando 2012). The dissipation term acts as a sink for TKE. Taken together, the terms on the right side of Eq. (65) determine whether the total TKE increases ($\frac{dK}{dt} > 0$) or decreases ($\frac{dK}{dt} < 0$). Traditionally, to obtain turbulent diffusivity, a steady state of turbulence ($\frac{d}{dt} \approx 0$, the tendency and advection terms are neglected) is assumed to exist. In steady state, the production term P is divided into J_b and ε; thus, the TKE equation can be presented as

$$0 = -\overline{u'w'}\frac{\partial \bar{u}}{\partial z} - g\frac{\overline{\rho'w'}}{\bar{\rho}} - \varepsilon = P - J_b - \varepsilon. \tag{67}$$

The ratio between P and J_b is the flux Richardson number:

$$R_f = \frac{\left(\frac{g}{\bar{\rho}}\right)\overline{\rho'u'}}{-\overline{u'w'}\frac{\partial \bar{u}}{\partial z}} = \frac{J_b}{P}. \tag{68}$$

In stably stratified fluids ($\frac{\partial \bar{\rho}}{\partial z} < 0$), R_f indicates how much TKE (K) is consumed to mix the stably stratified fluid (J_b). The remainder of the term P is dissipated by viscosity.

A.2 Eddy diffusivity

Vertical eddy diffusivity of density K_ρ is used in the calculation of vertical density flux F_ρ.

$$F_\rho = \overline{\rho'w'} = -\mathrm{K}_\rho\frac{\partial \bar{\rho}}{\partial z}, \tag{69}$$

where $\frac{\partial \bar{\rho}}{\partial z}$ is the background density gradient. Using Eqs. (67, 68, and 69), we can obtain an expression for K_ρ under a steady-state condition as follows (Osborn 1980):

$$K_\rho = \Gamma^{\mathrm{CT}}\frac{\varepsilon}{N^2}, \text{ where } \Gamma^{\mathrm{CT}} = \frac{R_f}{1-R_f} = \frac{J_b}{P-J_b} = \frac{J_b}{\varepsilon}, \; N = \sqrt{-\frac{g}{\rho_0}\left(\frac{\partial \bar{\rho}}{\partial z}\right)}. \tag{70}$$

ε can be measured by microstructure profilers such as the TurboMAP (e.g., Nakano et al. 2014), and N can be estimated using CTD measurements. If we know R_f, we can estimate K_ρ accurately. However, it is difficult to measure R_f. Osborn (1980) proposed 0.2 as a value for Γ^{CT} on the grounds that the critical value of R_f is about 0.15 in the Kelvin–Helmholtz billow.

Γ^{CT} is traditionally called the mixing efficiency for CT (e.g., Oakey 1985), but it is actually a mixing coefficient (Gregg et al. 2018; Kantha and Luce 2018). From Eqs. (68 and 67), it is determined that R_f is the rate of conversion of turbulent energy produced (from various energy sources) to buoyancy energy needed to mix stratification layers, and Γ^{CT} is simply the ratio of consumed buoyancy energy to energy dissipation by viscosity. Hereafter, Γ^{CT} is called the mixing coefficient (Gregg et al. 2018; Kantha and Luce 2018).

Temperature and salinity variance equations are given by

$$\frac{\mathrm{d}}{\mathrm{d}t}\left(\overline{T'^2}\right) = -\frac{\partial}{\partial x_j}\left[\overline{\left(u_j' T_j'^2\right)} - \left(k_T \frac{\overline{\partial T'^2}}{\partial x_j}\right)\right] - 2\overline{u_j' T'}\frac{\partial \bar{T}}{\partial x_j} - 2k_T \frac{\overline{\partial T'}}{\partial x_j}\frac{\overline{\partial T'}}{\partial x_j},$$
$$\frac{\mathrm{d}}{\mathrm{d}t}\left(\overline{T'^2}\right) = -\frac{\partial}{\partial x_j}(D_T) - 2\overline{u_j' T'}\frac{\partial \bar{T}}{\partial x_j} - 2k_T \frac{\overline{\partial T'}}{\partial x_j}\frac{\overline{\partial T'}}{\partial x_j}. \tag{71}$$

$$\frac{\mathrm{d}}{\mathrm{d}t}\left(\overline{S'^2}\right) = -\frac{\partial}{\partial x_j}\left[\overline{\left(u_j' S_j'^2\right)} - \left(k_S \frac{\overline{\partial S'^2}}{\partial x_j}\right)\right] - 2\overline{u_j' S'}\frac{\partial \bar{S}}{\partial x_j} - 2k_S \frac{\overline{\partial S'}}{\partial x_j}\frac{\overline{\partial S'}}{\partial x_j},$$
$$\frac{\mathrm{d}}{\mathrm{d}t}\left(\overline{S'^2}\right) = -\frac{\partial}{\partial x_j}(D_S) - 2\overline{u_j' S'}\frac{\partial \bar{S}}{\partial x_j} - 2k_S \frac{\overline{\partial S'}}{\partial x_j}\frac{\overline{\partial S'}}{\partial x_j}. \tag{72}$$

Here, k_T is the molecular diffusivity of heat (= 1.5×10^{-7} m^2/s at 20 °C and 34 PSU), and k_S is the molecular diffusivity of salt (= 1.5×10^{-9} m^2/s at 20 °C and 34 PSU). Note that k_T and k_S vary with temperature and salinity. The terms D_T and D_S are defined as

$$D_T = \underbrace{\overline{\left(u_j' T_j'^2\right)}}_{\text{Transport of temperature variance}} \quad \underbrace{-k_T \frac{\overline{\partial T'^2}}{\partial x_j}}_{\text{Molecular diffusion of temperature variance.}} \tag{73}$$

$$D_S = \underbrace{\overline{\left(u_j' S_j' 2\right)}}_{\text{Transport of salinity variance}} \quad \underbrace{-k_S \frac{\overline{\partial S'^2}}{\partial x_j}}_{\text{Molecular diffusion of salinity variance.}} \tag{74}$$

The terms $-\frac{\partial}{\partial x_j}(D_T)$ and $-\frac{\partial}{\partial x_j}(D_S)$ are also the diffusion of temperature and salinity variances and are considered to be small and negligible in a steady-state condition. Under the isotropic condition, we sum Eqs. (71 and 72), and obtain

$$0 = -\overline{w'T'}\frac{\partial \overline{T}}{\partial z} - \frac{1}{2}\chi_T \therefore \chi_T = 6k_T \overline{\left(\frac{\partial T'}{\partial z}\right)^2} \left[^\circ\mathrm{C}^2/\mathrm{s}\right], \tag{75}$$

$$0 = -\overline{w'S'}\frac{\partial \overline{S}}{\partial z} - \frac{1}{2}\chi_S \therefore \chi_S = 6k_S \overline{\left(\frac{\partial S'}{\partial z}\right)^2} \left[\mathrm{PSU}^2/\mathrm{s}\right]. \tag{76}$$

Here, $\frac{\partial \overline{T}}{\partial z}$ and $\frac{\partial \overline{S}}{\partial z}$ are the background temperature and salt gradients, respectively, and χ_T and χ_S are the dissipation rate of variances of turbulence temperature and salt gradients diffused by the molecular process, respectively. From the equation of state, we define

$$\rho = \rho_0\{1 - \alpha(\bar{T} - T_0 + T') + \beta(\bar{S} - S_0 + S')\}, \tag{77}$$

where a subscript 0 indicates a reference value. α and β take values as $\alpha = 2.62 \times 10^{-4}$/ °C and $\beta = 7.62 \times 10^{-4}$/ PSU, 20 °C, and 34PSU. Note that α and β vary with temperature and salinity. The density flux $\overline{\rho' w'}$ can then be written as

$$\rho' = \rho - \bar{\rho} = -\rho_0 \alpha T' + \rho_0 \beta S' \therefore \overline{\rho' w'} = \rho_0\left(-\alpha \overline{w'T'} + \beta \overline{w'S'}\right). \tag{78}$$

Putting Eq. (78) into Eq. (67), we obtain

$$0 = -\overline{u'w'}\frac{\partial \bar{u}}{\partial z} + g\left(\alpha \overline{w'T'} - \beta \overline{w'S'}\right) - \varepsilon. \tag{79}$$

The vertical fluxes of heat and salt (F_T and F_S) can then be written as

$$F_T = \overline{w'T'} = -K_T \frac{\partial \bar{T}}{\partial z}, \tag{80}$$

$$F_S = \overline{w'S'} = -K_S \frac{\partial \bar{S}}{\partial z}, \tag{81}$$

where K_S and K_T are the eddy diffusivity of salt and heat, respectively. From Eqs. (69, 78, 80, and 81), F_ρ is

$$F_\rho = -\rho_0 \alpha F_T + \rho_0 \beta F_S. \tag{82}$$

For a fully developed CT, K_T, K_S, and K_ρ must be equal to one another:

$$K_T = K_S = K_\rho. \tag{83}$$

K_T is derived using Eqs. (75 and 80) such that

$$K_T = \frac{\chi_T}{2\left(\frac{\partial \overline{T}}{\partial z}\right)^2} = \frac{3k_T \overline{\left(\frac{\partial T'}{\partial z}\right)^2}}{\left(\frac{\partial \overline{T}}{\partial z}\right)^2} \therefore K_T = k_T C_x = K_\rho, \tag{84}$$

where

$$C_x = 3\overline{\left(\frac{\partial T'}{\partial z}\right)^2} \Big/ \left(\frac{\partial \overline{T}}{\partial z}\right)^2 \tag{85}$$

is the Cox number (Osborn and Cox 1972), which represents the ratio of the variance of temperature gradient fluctuations to the square of the mean temperature gradient. The method by which one estimates K_T is known as the Osborn-Cox method.

Under the assumption of equality among all eddy diffusivities (Eq. 83), Γ^{CT} can be expressed using Eqs. (70 and 84) as follows:

$$\Gamma^{\mathrm{CT}} = \frac{R_f}{1 - R_f} = \frac{\chi_T N^2}{2\varepsilon\left(\frac{\partial \overline{T}}{\partial z}\right)^2}. \tag{86}$$

The quantities on the right-hand side of Eq. (86) can be measured by a microstructure profiler. Therefore, it is possible to estimate Γ^{CT}, with its estimated value being

0.265 (Oakey 1982, 1985). Moum (1996) obtained a value for Γ^{CT} in the range of 0.25–0.33. Thus, R_f is found to range between 0.2 and 0.25 when using these specified values. Using these values, one-fifth to one-fourth of TKE is converted into potential energy of the system. Also, CT changes the prevailing stratification. From Eq. (86), R_f can be written as

$$R_f = \frac{\chi_T N^2}{2\varepsilon\left(\frac{\partial \overline{T}}{\partial z}\right)^2 + \chi_T N^2}. \tag{87}$$

Thus, R_f can be estimated from microstructure measurements. Eddy diffusivity of momentum K_υ is defined as

$$-\overline{u'w'} = K_\upsilon \frac{\partial \bar{u}}{\partial z}. \tag{88}$$

Using Eq. (88), R_f can also be written as (St. Laurent and Schmitt 1999)

$$R_f = \frac{g\overline{\rho' w'}}{-\rho_0 \overline{u'w'}\frac{\partial \bar{u}}{\partial z}} = \frac{-K_\rho \frac{g}{\rho_0}\frac{\partial \bar{\rho}}{\partial z}}{K_\upsilon\left(\frac{\partial \bar{u}}{\partial z}\right)^2} = \frac{K_\rho}{K_\upsilon}\frac{N^2}{\left(\frac{\partial \bar{u}}{\partial z}\right)^2} = \frac{K_\rho}{K_\upsilon}R_i, \tag{89}$$

where R_i is the gradient Richardson number:

$$R_i = N^2 \Big/ \left(\frac{\partial \bar{u}}{\partial z}\right)^2. \tag{90}$$

Note that when $R_i < 0.25$, the fluid layer can become turbulent. Equation 89 can be rewritten as

$$\frac{R_i}{R_f} = \frac{K_\upsilon}{K_\rho} = \Pr_t, \tag{91}$$

where $\Pr_t$ is the turbulent Prandtl number. If R_f is determined from Eq. (87) and R_i is measured from background shear and stratification, from the diffusivity of momentum, K_υ can be estimated if K_ρ is known. In any case, it is important to recognize that R_f and the resultant Γ are not constants but depend on the prevailing stratification, more specifically as a function of R_i.

R_{eb} is defined as

$$R_{eb} = \frac{\varepsilon}{\upsilon N^2}. \tag{92}$$

From Eq. 66, R_{eb} represents the ratio of the variance of velocity gradient fluctuation to the stabilizing stratification. It is derived from the typical length and velocity scales based on ε and N as $L_B = (\varepsilon/N^3)^{1/2}$, $U_B = (\varepsilon/N)^{1/2}$. R_{eb} can be defined as $R_{eb} = \frac{U_B L_B}{\upsilon} = \frac{\varepsilon}{\upsilon N^2}$ (Gregg and Sanford 1988). Inoue et al. (2007) used R_{eb} for discriminating DDC from turbulence ($R_{eb} < 20$, CT is depressed, a nd DDC prevails, from Yamazaki, 1990). See Kantha and Luce (2018) for the significance of R_{eb}.

Appendix B Laboratory flux law

B.1 Salt finger convection (SF)

Salt finger convection (SF) can effectively transport salt and heat downward. The net downward density flux due to salt βF_S is larger than the net downward density flux due to the heat αF_T (F_S: vertical salt flux, F_T: vertical heat flux). The results show a decrease in total potential energy in the SF layer. This is in contrast to CT, in which the total potential energy increased. A threshold in the existence of SF is defined as $1 < R_\rho < 100$ (Turner 1967; Baines and Gill 1969).

From the linear stability treatment of SF, Stern (1975) and Kunze (1987) obtained the density flux ratio $\gamma^{SF} = \alpha F_T/\beta F_S$ (< 1) for the fastest-growing SF as

$$\gamma^{SF} = \sqrt{R_\rho}\left(\sqrt{R_\rho} - \sqrt{R_\rho - 1}\right) \tag{93}$$

Kelley (1986) compiled γ^{SF} as a function of R_ρ from laboratory data on SF:

$$\gamma^{SF} = 0.35\exp\left[1.05\exp\left(-2.16\left(R_\rho - 1\right)\right)\right] \tag{94}$$

The laboratory flux ratios and the numerically and theoretically determined ratios are shown in Fig. 6; γ^{SF} asymptotes to a constant value as R_ρ becomes large ($\sim$ 0.5: Eq. 93, $\sim$ 0.35: Eq. 94) (together with Polzin et al. 1995; Shen 1993, 1995; Taylor and Buscens 1989).

Buoyancy fluxes of salt and heat for SF are summarized by Kelley (1986):

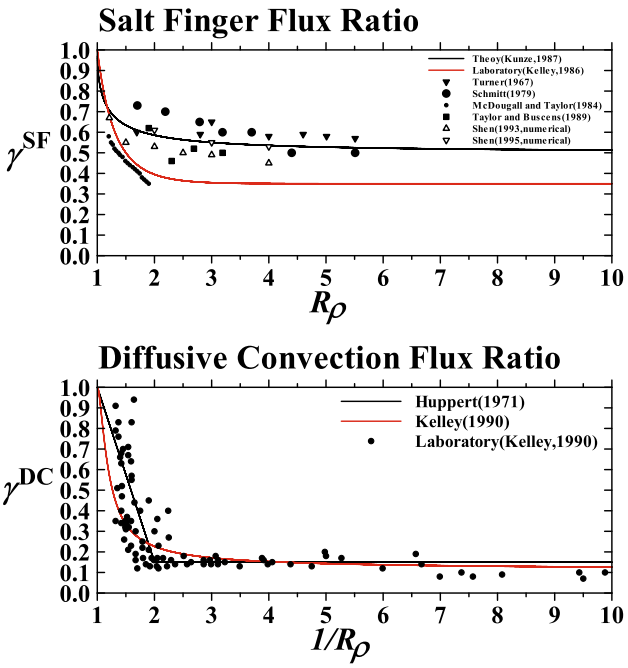

Fig. 6 DDC flux ratio dependence on R_ρ in which solid lines are theoretically or laboratory determined flux laws. Some laboratory and experimental numerical data are also shown for comparison

$$g\beta F_S = C_1 k_T^{1/3} (g\beta\Delta S)^{\frac{4}{3}}, C_1 = 0.04 + 0.327 R_\rho^{-1.91}, \quad (95)$$

$$g\beta F_T = \gamma^{\mathrm{SF}} g\beta F_S, \quad (96)$$

where ΔS is the salinity difference across the SF interface. Equations (95 and 96) are called Turner's 4/3 flux law. Kunze (1987) presented another set of flux laws for SF which depend on whether SF developed in thick or thin interfaces; for thick interfaces (> 1 m):

$$g\beta F_S = 2\upsilon g\beta \frac{\partial \bar{S}}{\partial z}\left[R_\rho^{\frac{1}{2}} + \left(R_\rho - 1\right)^{\frac{1}{2}}\right]^2, \quad g\beta F_T = \gamma^{\mathrm{SF}} g\beta F_S, \quad (97)$$

and for thin interfaces (< 1 m):

$$g\beta F_S = \frac{1}{8} k_T^{1/3} (g\beta\Delta S)^{\frac{4}{3}}, \quad g\alpha F_T = \gamma^{\mathrm{SF}} g\beta F_S. \quad (98)$$

Another estimate of buoyancy flux comes from the "collective instability of SF" argued by Stern (1969). The author considered the interaction of SF with a large-scale IW that resulted in the tilting of SF due to vertical velocity shear. As a result, vertical fluxes change their direction, causing a divergence or convergence of fluxes, changes in density and velocity fields, and a collapse of SF. The critical condition of collapse is presented by the non-dimensional Stern number, S_t:

$$S_t = \frac{(\beta F_S - \alpha F_T)}{\upsilon(\alpha\partial\bar{T}/\partial z - \beta\partial\bar{S}/\partial z)} = \frac{g(\beta F_S - \alpha F_T)}{\upsilon N^2} = \frac{\beta F_S(1-\gamma^{\mathrm{SF}})}{\upsilon\beta\bar{S}_z(R_\rho - 1)} \approx 1. \quad (99)$$

$\frac{\partial\bar{T}}{\partial z}$ is the vertical salt gradient. If S_t becomes larger than unity, the transport of energy to large-scale IW overcomes viscous dissipation, and the SF collapses. From this equation, the vertical transport of salt is estimated as:

$$\beta F_S = \frac{S_t\upsilon(R_\rho - 1)}{(1-\gamma^{\mathrm{SF}})}\beta\frac{\partial\bar{S}}{\partial z}. \quad (100)$$

As determined in the laboratory, the value of S_t varies from 1 (Schmitt 1979) to 4 (McDougall and Taylor 1984). Based on flux estimation, K_S^{SF} and K_T^{SF} for SF can be obtained as:

$$F_S = -K_S^{\mathrm{SF}}\frac{\partial\bar{S}}{\partial z} \therefore K_S^{\mathrm{SF}} = -\frac{F_S}{\partial\bar{S}/\partial z}, \quad F_T = -K_T^{\mathrm{SF}}\frac{\partial\bar{T}}{\partial z} \therefore K_T^{\mathrm{SF}} = -\frac{F_T}{\partial\bar{T}/\partial z}. \quad (101)$$

B.2 Diffusive convection (DC)

For diffusive convection (DC), salt and heat are transported upward. Moreover, the net downward density flux due to αF_T is larger than that due to βF_S. The density flux ratio for DC is defined as $\gamma^{\mathrm{DC}} = \beta F_S/\alpha F_T$ (< 1) (Turner, 1965). For DC, net density transport is downward and increases the density in the lower layer. The threshold of existence for DC is $0 < R_\rho < 1$. Huppert (1971) and Kelley (1990) obtained the following relations for γ^{DC} as a function of R_ρ for DC using laboratory data: Huppert (1971) introduced

$$\gamma^{\mathrm{DC}} = \begin{cases} 1.85 - 0.85R_\rho^{-1} & \text{for } 0.5 < R_\rho < 1 \\ 0.15 & \text{for } R_\rho < 0.5 \end{cases}, \quad (102)$$

and Kelley (1990) introduced

$$\gamma^{\mathrm{DC}} = \frac{R_\rho^{-1} + 1.4\left(R_\rho^{-1} - 1\right)^{3/2}}{1 + 14\left(R_\rho^{-1} - 1\right)^{3/2}}. \quad (103)$$

Thus, γ^{DC} becomes 1 for R_ρ= 1, and becomes a constant ($\sim$ 0.15: Eq. 102, $\sim$ 0.13: Eq. 103, see Fig. 6) as R_ρ decreases. Individual fluxes of salt and heat for DC were summarized by Kelley (1986, 1990) as the following:

$$g\beta F_S = \gamma^{\mathrm{DC}} g\alpha F_T, \quad g\alpha F_T = C_2\left(k_T/\upsilon\right)^{\frac{1}{3}}(g\alpha\Delta T)^{\frac{4}{3}}, C_2 = 0.0032\exp\left(4.8R_\rho^{0.72}\right). \quad (104)$$

ΔT is the temperature difference across the DC interface. Eddy diffusivities for salt and heat for DC (K_S^{DC} and K_T^{DC}) are formulated in the same way as Eq. (101).

Appendix C SMC model (Kantha 2012)

Kantha (2012) and Kantha et al. (2011) introduced conservation equations for the TKE, temperature, and salinity variances $\overline{u'v'} = 0$, $\overline{v'w'} = 0$, $\overline{v'T'} = 0$, $\overline{v'S'} = 0$ as follows:

$$\overline{u'w'} + \lambda_4\tau g\alpha\overline{u'T'} - \lambda_4\tau g\beta\overline{u'S'}, \quad (105)$$

$$\overline{u'T'} = -\frac{\tau}{\lambda_5}\left(\overline{u'w'}\frac{\partial\bar{T}}{\partial z} + \frac{1}{2}(\lambda_6 + \lambda_7)\overline{w'T'}\frac{\partial\bar{u}}{\partial z}\right) \quad (106)$$

$$\overline{u'S'} = -\frac{\tau}{\lambda_9}\left(\overline{u'w'}\frac{\partial\bar{S}}{\partial z} + \frac{1}{2}(\lambda_6 + \lambda_7)\overline{w'S'}\frac{\partial\bar{u}}{\partial z}\right) \quad (107)$$

$$\overline{w'T'} = -\frac{\tau}{\lambda_5}\left\{\overline{w'2}\frac{\partial\bar{T}}{\partial z} - g\left[-\lambda_8\tau\overline{w'T'}\alpha\frac{\partial\bar{T}}{\partial z} + \lambda_{11}\tau\left(\overline{w'T'}\beta\frac{\partial\bar{S}}{\partial z} + \overline{w'S'}\beta\frac{\partial\bar{T}}{\partial z}\right)\right]\right\} \quad (108)$$

$$\overline{w'S'} = -\frac{\tau}{\lambda_9}\left\{\overline{w'2}\frac{\partial\bar{S}}{\partial z} - g\left[-\lambda_{11}\tau\left(\overline{w'T'}\alpha\frac{\partial\bar{S}}{\partial z} + \overline{w'S'}\alpha\frac{\partial\bar{T}}{\partial z}\right) + \lambda_{10}\tau\overline{w'S'}\beta\frac{\partial\bar{S}}{\partial z}\right]\right\} \tag{109}$$

Using closure modeling developed by Galperin et al. (1988), one can obtain estimates for variances of temperature and salinity as well as covariance between temperature and salinity as follows:

$$\overline{T'^2} = -\frac{\lambda_8\tau}{\lambda_0}\overline{w'T'}\frac{\partial\bar{T}}{\partial z}, \tag{110}$$

$$\overline{S'^2} = -\frac{\lambda_{10}\tau}{\lambda_0}\overline{w'S'}\frac{\partial\bar{S}}{\partial z}, \tag{111}$$

$$\overline{T'S'} = -\frac{\lambda_{10}\tau}{\lambda_0}\left[\overline{w'T'}\frac{\partial\bar{S}}{\partial z} + \overline{w'S'}\frac{\partial\bar{T}}{\partial z}\right]. \tag{112}$$

where λs are closure constants $\lambda_1 = 0.1239$, $\lambda_2 = \lambda_3 = \lambda_4 = 0.1050$, $\lambda_5 = \lambda_9 = 8.9209$, $\lambda_6 = \lambda_7 = 0.5709$, $\lambda_8 = \lambda_{10} = 0.5801$, and $\lambda_{11} = 0.27$. Closure constants for CT are

$$\begin{aligned}\widetilde{\lambda_5} &= \lambda_5[1 + R_i],\\ \widetilde{\lambda_9} &= 0.02\lambda_9[1 + R_i].\end{aligned} \tag{113}$$

Those for DDC are defined as

$$\begin{aligned}\widehat{\lambda_5} &= 0.02\lambda_5\left[1 + 6.5\left(R_\rho^{-1}\right)^{5/4}\right],\\ \widehat{\lambda_9} &= 0.02\lambda_9\left[1 + 6.5\left(R_\rho\right)^{5/4}\right],\\ \widehat{\lambda_{11}} &= \lambda_{11}\left(\frac{2}{R_\rho + R_\rho^{-1}}\right).\end{aligned} \tag{114}$$

Those for the combination of CT and DDC are defined as

$$\begin{aligned}\overline{\lambda_5} &= \widetilde{\lambda_5}[1 - f(R_i)] + \widehat{\lambda_5}[f(R_i)],\\ \overline{\lambda_9} &= \widetilde{\lambda_9}[1 - f(R_i)] + \widehat{\lambda_9}[f(R_i)],\\ \overline{\lambda_{11}} &= \widetilde{\lambda_{11}}[1 - f(R_i)] + \widehat{\lambda_{11}}[f(R_i)].\end{aligned} \tag{115}$$

Appendix D Terminology

D.1 Acronyms and abbreviations

ADCP	Acoustic Doppler current profiler
C-SALT	Caribbean sheets and layers transect
CT	Conventional turbulence
CTD	Conductivity temperature depth profiler
DC	Diffusive convection
DDC	Double-diffusive convection
DNS	Direct numerical simulations
EM-APEX	Electromagnetic autonomous profiling explorer
HRP	High-resolution profiler
IW	Internal wave
KPP	K-profile parameterization
LADCP	Lowered ADCP
Meddy	Mediterranean eddy
MOC	Meridional overturning circulation
NATRE	North Atlantic Tracer Release Experiment
PSU	Practical salinity unit
SF	Salt finger
SMC	Second-moment closure
TKE	Turbulent kinetic energy
TurboMAP	Turbulence ocean microstructure acquisition profiler

D.2 Symbols

Greek symbols

α	Expansion coefficient due to heat [= 2.62×10^{-4}/ °C, 20 °C and 34 PSU]
$\alpha\, F_T$	Density flux of heat [m/s]
$\alpha\frac{\partial\bar{T}}{\partial z}$	Background density gradient due to temperature
β	Contraction coefficient due to salinity [= 7.62×10^{-4}/PSU, 20 °C, 34 PSU]
$\beta\, F_S$	Density flux of salt [m/s]
$\beta\frac{\partial\bar{S}}{\partial z}$	Background vertical density gradient due to salt [1/m]
Γ^{CT}	Mixing coefficient for CT [non-dimensional]
Γ^{DDC}	Mixing coefficient for DDC [non-dimensional]
Γ^{SF}	Mixing coefficient for SF [non-dimensional]
Γ^{DC}	Mixing coefficient for DC [non-dimensional]
γ^{SF}	Density flux ratio of SF [non-dimensional]
γ^{DC}	Density flux ratio of DC [non-dimensional]
ΔS	Salinity difference across SF interface [PSU]
ΔT	Temperature difference across DC interface [°C]
ε	Kinetic energy dissipation rate [W/kg]
$\lambda_1 \sim \lambda_{11}$	Closure constants
υ	Kinematic molecular viscosity [$\sim 1.05 \times 10^{-6}$ m^2/s at 20 °C and 34 PSU]
ρ	Density [kg/m^3]
ρ'	Fluctuation density [kg/m^3]
$\bar{\rho}$	Mean density [kg/m^3]
ρ_0	Reference density [kg/m^3]
τ	Timescale of turbulence dissipation [s]
χ_S	Dissipation rate of salt variance [PSU^2/s]
χ_T	Dissipation rate of temperature variance [°C^2/s]

English symbols

B_1 Coefficient for turbulent timescale [non-dimensional]

C_1 Coefficient of Turner's 4/3 flux law [non-dimensional]

C_{SMC} Parameter used in second closure constants

C_x Cox number $\left[\left[= 3\overline{\left(\frac{\partial T'}{\partial z}\right)^2} \Big/ \left(\frac{\partial \overline{T}}{\partial z}\right)^2\right]\right.$, non-dimensional]

D_{ij} Energy transport by triple-correlation components [$\mathrm{m}^3/\mathrm{s}^3$]

D_S Diffusion of salt by triple-correlation components [$\mathrm{PSU}^2\mathrm{m/s}$]

D_T Diffusion of temperature by triple-correlation components [$^\circ\mathrm{C}^2\,\mathrm{m/s}$]

F_S Vertical salt flux [$\mathrm{PSU}\cdot\mathrm{m/s}$]

F_T Vertical heat flux [$^\circ\mathrm{C\,m/s}$]

F_ρ Vertical density flux [$\mathrm{kg\,m}^2/\mathrm{s}$]

G_T Square of the ratio of the turbulent timescale to the buoyancy timescale [non-dimensional]

G_υ Square of the ratio of the turbulent timescale to the shear timescale [non-dimensional]

g Gravitational acceleration [$\mathrm{m/s}^2$]

i, j Indices take the values 1, 2, and 3, which correspond to the x-, y-, and z-direction

J_b Energy production or dissipation via the turbulent density flux [W/kg]

K Turbulent kinetic energy ($= q^2/2$) [$\mathrm{m}^2/\mathrm{s}^2$]

K_b Background eddy diffusivity [m^2/s]

K_S Vertical eddy diffusivity of salt [m^2/s]

K_S^{DC} Vertical eddy diffusivity of salt for DC [m^2/s]

K_S^{SF} Vertical eddy diffusivity of salt for SF [m^2/s]

K_T Vertical eddy diffusivity of heat [m^2/s]

K_T^{SF} Vertical eddy diffusivity of heat for SF [m^2/s]

K_T^{DC} Vertical eddy diffusivity of heat for DC [m^2/s]

K_υ Vertical eddy diffusivity of momentum [m^2/s]

K_ρ Vertical eddy diffusivity of density [m^2/s]

K_ρ^{CT} Vertical eddy diffusivity of density for CT [m^2/s]

K_ρ^{DC} Vertical eddy diffusivity of density for DC [m^2/s]

K_ρ^{DDC} Vertical eddy diffusivity of density for DDC (indicates both K_ρ^{SF} and K_ρ^{DC}) [m^2/s]

K_ρ^{IW} Eddy diffusivities due to internal wave breaking [m^2/s]

K_ρ^{SF} Vertical eddy diffusivity of density for SF [m^2/s]

K_ρ^{Shear} Eddy diffusivities due to vertical shear instability [m^2/s]

k_S Molecular diffusivity of salt ($= 1.5 \times 10^{-9}$ m^2/s at 20 °C and 34 PSU)

k_T Molecular diffusivity of temperature ($= 1.5 \times 10^{-7}$ m^2/s at 20 °C and 34 PSU)

L_B Typical length scale of turbulence [m]

ℓ Turbulence length scale [m]

N Buoyancy frequency [1/s]

P Energy production of Reynolds stress against mean shear [W/kg]

Pr_t Turbulent Prandtl number [$= \frac{K_\upsilon}{K_\rho}$ non-dimensional]

p Pressure [$\mathrm{kg/(m\,s}^2)$]

$\bar{p}$ Mean pressure [$\mathrm{kg/(m\,s}^2)$]

p' Fluctuation pressure [$\mathrm{kg/(m\,s}^2)$]

q Turbulence velocity scale [m/s]

R_{eb} Buoyancy Reynolds number [$= \frac{\varepsilon}{\upsilon N^2}$, non-dimensional]

R_f Flux Richardson number $\left[= \frac{\left(\frac{g}{\rho}\right)\overline{\rho' w'}}{-\overline{u'w'}\frac{\partial \bar{u}}{\partial z}}\text{, non-dimensional}\right]$

R_i Gradient Richardson number $\left[= N^2 \Big/ \left(\frac{\partial \bar{u}}{\partial z}\right)^2\text{, non-dimensional}\right]$

R_ρ Density ratio, the ratio of the background density gradient due to temperature to that of salt [$= \alpha \bar{T}_z/\beta \bar{S}_z$ non-dimensional]

S Salinity [PSU]

$\bar{S}$ Mean salinity [PSU]

S' Salinity fluctuation [PSU]

$\overline{S'^2}$ Variance of salt fluctuation [PSU^2]

S_t Stern number [$= \frac{(\beta F_S - \alpha F_T)}{\upsilon(\alpha \partial \bar{T}/\partial z - \beta \partial \bar{S}/\partial z)}$, non-dimensional]

S_S Structure function for salt diffusivities [non-dimensional]

S_T Structure function for heat diffusivities [non-dimensional]

S_υ Structure function for the momentum diffusivities [non-dimensional]

S_ρ Structure function for density diffusivities [non-dimensional]

T Temperature [°C]

T' Temperature fluctuation [°C]

$\bar{T}$ Mean temperature [°C]

$\overline{T'^2}$ Variance of temperature fluctuation [$^\circ\mathrm{C}^2$]

$\overline{T'S'}$ Covariance between temperature and salinity fluctuations [$^\circ\mathrm{C\,PSU}$]

t Time [s]

U_B Typical turbulence velocity scale [m/s]

u_i Velocity [m/s]. i takes the vales 1, 2, and 3, which correspond to the x-, y-, and z-direction. (u_1, u_2, u_3) = (u, v, w)

$\bar{u}$ Mean velocity in x-direction [m/s]

u' Turbulence velocity in x-direction [m/s]

$\overline{u'w'}$ Turbulence momentum transport [$\mathrm{m}^2/\mathrm{s}^2$]

$\bar{v}$ Mean velocity in y-direction [m/s]

v'	Turbulence velocity in y-direction [m/s]
$\bar{w}$	Mean velocity in z-direction [m/s]
w'	Turbulence velocity in z-direction [m/s]
$\overline{w'S'}$	Turbulence salt transport [PSU m/s]
$\overline{w'T'}$	Turbulence heat transport [°C m/s]
x	Horizontal coordinate positive eastward
y	Horizontal coordinate positive northward
z	Vertical coordinate positive upward

Mathematical symbols

δ_{ij}	Kronecker delta ($\delta_{ij} = 1$ when $i = j$, $\delta_{ij} = 0$ when $i \neq j$)
$\frac{\partial \bar{S}}{\partial z}$	Background salt gradient [PSU/m]
$\frac{\partial \bar{T}}{\partial z}$	Background temperature gradient [°C/m]
$\frac{\partial \bar{u}}{\partial z}$	Background velocity shear [1/s]
$\overline{\left(\frac{\partial u'}{\partial z}\right)^2}$	Variance of turbulence velocity shear [$1/s^2$]
$\overline{\left(\frac{\partial T'}{\partial z}\right)^2}$	Variance of turbulence temperature gradient [$(°C/m)^2$]
$\overline{\left(\frac{\partial S'}{\partial z}\right)^2}$	Variance of turbulence salt gradient [$(PSU/m)^2$]
$\frac{\partial \bar{\rho}}{\partial z}$	Background vertical density gradient [kg/m^4]
$\frac{\partial^2 \rho}{\partial z^2}$	The second derivative of density [kg/m^5]
[-]	Denotes ensemble average of turbulence component

References

Baines WD, Gill AE (1969) On thermohaline convection with the linear gradient. J Fluid Mech 37:289–306

Bryan FO (1987) Parameter sensitivity of primitive equation ocean general circulation models. J Phys Oceanogr 17:970–985

Canuto VM, Cheng Y, Howard A (2008) A new model for double diffusion + turbulence. Geophys Res Lett 35:L02613. https://doi.org/10.1029/2007GL032580

de Lavergne C, Madec G, Le Sommer A, Naveira Garabato AC (2016) The impact of a variable mixing efficiency on the abyssal overturning. J Phys Oceangr 46:663–681

Galperin B, Kantha L, Hassid S, Rosati A (1988) A quasi-equilibrium turbulent energy model for geophysical flows. J Atomos Sci 45:55–62

Gargett AE (1984) Vertical eddy diffusivity in the ocean interior. J Mar Res 42:359–393

Gargett AE, Holloway G (1984) Dissipation and diffusion by internal wave breaking. J Mar Res 42:15–27

Gargett AE, Holloway G (1992) Sensitivity of the GFDL ocean model to different diffusivities for heat and salt. J Phys Oceanogr 22:1158–1177

Gregg MC (1989) Scaling turbulent dissipation in the thermocline. J Geophys Res 94:9686–9698

Gregg MC, Sanford T (1988) The dependence of turbulent dissipation on stratification in a diffusively stable thermocline. J Geophys Res 93:12381–12392

Gregg MC, D'Asaro EA, Riley JJ, Kunze E (2018) Mixing efficiency in the ocean. Ann Rev Mar Sci 10:1

Hinze JO (1975) Turbulence. McGraw-Hill, New York, p 790

Hirano D, Kitade Y, Nagashima H, Matsuyama M (2010) Characteristics of observed turbulent mixing across the Antarctic Slope Front at 140E, east Antarctica. J Oceanogr 66:95–104

Huppert HE (1971) On the stability of a series of double-diffusive layers. Deep Sea Res 18:1005–1021

Inoue R, Yamazaki H, Wolk F, Kono T, Yoshida J (2007) An estimation of buoyancy flux for a mixture of turbulence and double diffusion. J Phys Oceanogr 37:611–624

Inoue R, Kunze E, St Laurent L, Schmitt RW, Toole JM (2008) Evaluating salt-fingering theory. J Mar Res 66:413–440

Ishizu M, Kitade Y, Michida Y (2012) Mixing processes on the northeast coast of Hokkaido in summer. J Oceanogr. https://doi.org/10.1007/s10872-012-0152-6

Kantha L (2012) Modeling turbulent mixing in the global ocean: second moment closure models. In: Marcuso RJ (ed) Turbulence: theory, types and simulation, chapter 1. Nova Science Publisehers, New York, pp 1–68

Kantha L, Carniel S (2009) A note on modeling mixing in stably stratified flows. J Atmos Sci 66:2501–2505

Kantha L, Luce H (2018) Mixing coefficient in stably stratified flows. J Phys Oceanogr 48:2649–2665

Kantha L, Carniel S, Sclavo M (2011) A note on modeling double diffusive mixing in the global ocean. Ocean Model 36:40–48

Karl DM (1999) A sea of change: biogeochemical variability in the north Pacific subtropical Gyre. Ecosystems 2:181–214

Kelley D (1984) Effective diffusivities within oceanic thermohaline staircases. J Geophys Res 89:10484–10488

Kelley D (1986) Oceanic thermocline staircase. Ph.D. Thesis, Dalhousie University, Halifax, NS, Canada

Kelley D (1990) Fluxes through diffusive staircases: a new formulation. J Geophys Res 95(C3):3365–3371

Kimura S, Smyth W, Kunze E (2011) Turbulence in a sheared salt-fingering-favorable environment: anisotrophy and effective diffusivities. J Phys Oceanogr 41:1144–1159

Kunze E (1987) Limits on growing, finite length salt fingers: a Richardson number constraint. J Mar Res 45:533–556

Kunze E (1990) The evolution of salt fingers in inertial wave shear. J Mar Res 48:471–504

Large WG, McWilliams JC, Doney SC (1994) Oceanic vertical mixing: a review and a model with a nonlocal boundary layer parameterization. Rev Geophys 32:363–403

Linden PF (1974) Salt fingers in a steady shear flow. Geophys Fluid Dyn 6:1–27

Lozovatsky ID, Fernando HJS (2012) Mixing efficiency in natural flows. Phill Trans R Soc A. https://doi.org/10.1098/rsta.2012.0213

Marmorino GO, Caldwell DR (1976) Heat and salt transport through a diffusive thermohaline interface. Deep Sea Res 23:59–67

McDougall TJ, Taylor JR (1984) Flux measurements across a finger interface at a low value of stability ratio. J Mar Res 42:1–14

Merryfield W, Holloway G, Gargett AE (1999) A global ocean model with double-diffusive mixing. J Phys Oceangr 29:1124–1142

Moum JN (1996) Efficiency of mixing in main thermocline. J Geophys Res 101:12057–12069

Munk WH (1966) Abbyssal recipes. Deep Sea Res 13:707–730

Nagai T, Inoue R, Tandon A, Yamazaki H (2015) Evidence of doubule diffusive-convection below the main stream of Kuroshio Extension. J Geophys Res Oceans 120:8402–8421. https://doi.org/10.1002/2015JC011288

Nagasaka M, Yoshida J, Nagashima H, Matsuyama M, Kawasaki K, Yokouchi K (1999) On the double diffusive intrusion observed in the Oyashio frontal region. Theor Appl Mech 48:393–408

Nagata Y (1970) Detailed temperature cross section of the cold water belt along the northern edge of the Kuroshio. J Mar Res 28:1–14
Nakano H (2016) Parameterization of mixing in the ocean: double diffusive convection, turbulent eddies, and dissipation ratio. Ph.D Thesis Tokyo University of Marine Science and Technology
Nakano H, Shimada K, Nemoto M, Yoshida J (2014) Parameterization of the eddy diffusivity due to the double diffusive convection. Lamer 52:91–98
Oakey NS (1982) Determination of the rate of dissipation of turbulent energy from simultaneous temperature and velocity shear microstructure measurements. J Phys Oceanogr 12:256–271
Oakey NS (1985) Statistics of mixing parameters in the upper ocean during JASIN Phase 2. J Phys Oceanogr 15:1662–1675
Oakey NS (1988) Estimates of mixing inferred from temperature and velocity microstructure. In: Nihoul J, Jamart B (eds) Small-scale turbulence and mixing in the ocean, Elsevier oceanography series, vol 46. Elsevier, New York, pp 239–248
Osborn TR (1980) Estimates of the local rate of vertical diffusion from dissipation measurements. J Phys Oceanogr 10:83–89
Osborn TR, Cox CS (1972) Oceanic finestructure. Geophys Fluid Dyn 3:321–345
Polzin KL, Toole JM, Schmitt RW (1995) Finescale parameterizations of turbulent dissipation. J Phys Oceangr 25:306–328
Polzin KL, Toole JM, Ledwell JR, Schmitt RW (1997) Spatial variability of turbulent mixing in the abyssal ocean. Science 276(4):93–96
Radko T, Smith DP (2012) Equilibrium transport in double-diffusive convection. J Fluid Mech 692:5–27. https://doi.org/10.1017/jfm.2011.343
Schmitt RW (1979) Flux measurements on salt fingers at an interface. J Mar Res 37:419–436
Schmitt RW, Ledwell JR, Montgomery ET, Polzin KL, Toole JM (2005) Enhanced diapycnal mixing by salt fingers in the thermocline of the tropical Atlantic release experiment. Science 308:685–688
Shen CY (1993) Heat-salt fluxes across a density interface. Phys Fluids A5(11):2633–2643
Shen CY (1995) Equilibrium salt-fingering convection. Phys Fluids 7(4):706–717
St. Laurent L, Schmitt RW (1999) The contribution of salt fingers to vertical mixing in the North Atlantic tracer release experiment. J Phys Oceangr 29:1404–1424
Stern ME (1969) Collective instability of salt fingers. J Fluid Mech 35:209–218
Stern ME (1975) Ocean Circulation Physics. Academic Press, New York, p 243
Talley LD, Yun Y (2001) The role of cabbeling and double diffusion in setting the density of the North Pacific intermediate water salinity minimum. J Phys Oceanogr 31:1538–1549
Taylor JR, Buscens P (1989) Laboratory experiments on the structure of salt fingers. Deep Sea Res 36(11):1675–1704
Turner JS (1965) The coupled turbulent transports of salt and heat across a sharp density interface. Int J Heat Mass Transfer 8:759–767
Turner JS (1967) Salt fingers across a density interface. Deep Sea Res 14:599–611
Wells MG, Griffiths RW, Turner JS (2001) Generation of density fine structure by salt fingers in a spatially periodic shear. J Geophys Res 106(C4):7027–7036. https://doi.org/10.1029/2000JC000620
Yamazaki H (1990) Stratified turbulence near a critical dissipation rate. J Phys Oceanogr 20:1583–1598
Yih CS (1979) Fluid mechanics: a concise introduction to theory. West River Press, Ann Arbor, p 622
Zhang JR, Schmitt RW, Huang RX (1998) The sensitivity of the GFDL modular ocean model to parameterization of double - diffusive processes. J Phys Oceanogr 28:589–605